ERASMUS UNIVERSITY ROTTERDAM

MASTER'S THESIS

Integrating Battery Degradation in the Network Design for Electrical Buses with Fast Charging Technology

Author:
Jeroen VESTER
Student ID:
362010

Supervisor:
Dr. Shadi SHARIF AZADEH
Co-reader:
Dr. Krzysztof S. POSTEK

A thesis submitted in fulfillment of the requirements for the degree of Master of Science

in

ECONOMETRICS AND MANAGEMENT SCIENCE
Department of Econometrics
Erasmus School of Economics

October 12, 2018

ERASMUS UNIVERSITY ROTTERDAM

Declaration of Authorship

I, Jeroen VESTER, declare that this thesis titled, "Integrating Battery Degradation in the Network Design for Electrical Buses with Fast Charging Technology" and the work presented in it are my own. I confirm that:

- This work was done wholly or mainly while in candidature for a degree at this University.
- Where any part of this thesis has previously been submitted for a degree or any other qualification at this University or any other institution, this has been clearly stated.
- Where I have consulted the published work of others, this is always clearly attributed.
- Where I have quoted from the work of others, the source is always given. With the exception of such quotations, this thesis is entirely my own work.
- I have acknowledged all main sources of help.

Signed: 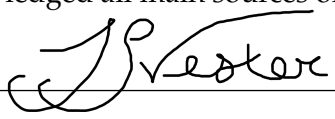

Date: 11-10-2018

ERASMUS UNIVERSITY ROTTERDAM

Abstract

Erasmus School of Economics
Department of Econometrics

Master of Science

Integrating Battery Degradation in the Network Design for Electrical Buses with Fast Charging Technology

by Jeroen VESTER

The reduction of greenhouse gas emissions is a major issue in worldwide governmental policy making. The transportation industry is responsible for a considerable part of greenhouse gas emissions. Electrification of the sector is a viable approach to reduce these emissions, as even electric cars powered by coal-generated electricity could cut emissions of the sector in half. In public transport electric transportation is currently mainly implemented with visually polluting catenary-powered trams or buses. Recent innovations in battery technology allow for public transport buses to be battery-driven and recharged at distinguished stops, rather than powered by catenary wires. Various trial projects have shown this technology is feasible for public transport operations and the contribution to gas emission control in urban areas is significant.

Creating a network for an electrical catenary-free public transport system is very costly due to their battery usage and installing high-tech charging stations. Cost optimization is therefore key for the promotion of battery-driven buses. In recent years, several papers have addressed designing such networks from technological as well as operational aspects. The operational decisions have a major impact on battery degradation in such systems. In order to achieve accurate cost optimization the maximization of battery life is crucial. In this paper, we introduce a linearized battery degradation model incorporated in an MILP for the design of such electrical public transport networks. Two commonly used approaches are applied for designing a Multicriteria Optimization Problem, weighted sum and ε-constraint.

A case study with semi-real data is conducted to compare the impact of incorporating battery aging on the costs and battery life with the results of a model without battery lifetime optimization.

Keywords: *Public Transportation, Tactical Design, Facility Planning, Mixed-Integer Programming, Mathematical Model, Network Design, Battery Degradation, Electric Bus, Multicriteria Optimization, Discrete Optimization*

Acknowledgements

I would first like to thank my thesis supervisor Dr. Shadi Sharif Azadeh of the Erasmus School of Economics at Erasmus University Rotterdam. She involved me in a project of her own research, introducing me to the field of academia. The door to Dr. Sharif Azadeh's office was always open whenever I had a question about my research or writing and she showed great support in difficult times. She consistently allowed this paper to be my own work, but steered me in the right the direction whenever she thought I needed it.

Finally, I must express my very profound gratitude to my parents and to my dear friends and boyfriend for providing me with unfailing support and continuous encouragement throughout my years of study and through the process of researching and writing this thesis. A special thanks goes to Charlotte Takken who has guided me greatly in the last year and stood there to help anytime. This accomplishment would not have been possible without these people. Thank you.

Jeroen Vester

Contents

List of Figures

List of Tables

List of Abbreviations

CB	**C**onventional (combustion engine) **B**us
CC	**C**onstant **C**urrent
CP	**C**onstant **P**ower
CV	**C**onstant **V**oltage
DOD	**D**epth **O**f **D**ischarge
EB	**E**lectric **B**us
EOL	**E**nd **O**f **L**ife
ESS	**E**nergy **S**torage **S**ystem
FFS	**F**ast **F**eeding **S**tation
GHG	**G**reen**h**ouse **G**as
Li-ion	**Li**thium-**ion**
MILP	**M**ixed **I**nteger **L**inear **P**rogramming
MOP	**M**ulticriteria **O**ptimization **P**roblem
NREL	**N**ational **R**enewable **E**nergy **L**aboratory
SFS	**S**tandard **F**eeding **S**tation
SOC	**S**tate **O**f **C**harge
TCO	**T**otal **C**ost (of) **O**wnership
TFS	**T**erminal **F**eeding **S**tation

List of Terminology

A brief explanation of frequently used terminology in this thesis.

battery cycle	The time between two consecutive recharges of a battery.
bus cycle	The time required for a round trip of a bus.
bus line	The route a bus operates on.
calendar lifetime	The time until a battery reaches its EOL capacity.
cycle lifetime	The number of battery cycles a battery can perform until it reaches its EOL capacity.
charging	Connecting a battery to energy supply to increase SOC
discharging	Using the energy stored in the battery
DOD	'Depth-of-discharge', the difference between minimum and maximum reached SOC on a day.
dwell time	The time a bus spends at a bus stop.
energy level/ battery level	The absolute amount of energy in a battery in kWh.
energy storage system	The device used for energy storage.
EOL	'End-of-life', when the capacity of a battery is reduced to a predefined fraction of its original capacity
fast/slow/terminal feeding station	The different types of charging stations.
NREL-model	Simulation tool from NREL to determine battery degradation.
round trip	The sequence of stops with the same start and end after which the sequence is repeated.
SOC	'State-of-charge', the relative amount of energy in a battery, expressed in % or as value between 0-1.
travel time	The time a bus spends for traveling between stops.

List of Symbols

	SETS	
$t \in T$	Set of charging station types, $\{FFS, SFS, TFS\}$	
$s \in S$	Set of stops, $\{1, \ldots, A\}$	
$d \in D$	Set of unique stops, regarding back and forth stops as one	
$s \in S^t$	Set of stops suitable for charging station type t	
$s \in S^d$	Back-forth stop pairs, $d \in D$, $S^d \subset S$	
$i \in I$	Set of battery sizes	
	PARAMETERS	
	Model parameters	
α_d^t	savings of both way installing charging station of type t at stop d	€
β	number of buses operated on the route	
γ_{batt}	marginal cost of battery	€/kWh
$\Gamma_{batt,i}$	total cost of battery configuration i ($\gamma_{batt} \cdot \kappa_i$)	€
Γ_s^t	cost of installing charging station of type t at stop s	€
δ_s	available dwell time at stop s	sec
δ_{depot}	available time at depot to charge overnight	sec
ε_{deg}	restriction on battery degradation in the ε-constraint method	
ζ	lower bound on the usable SOC, threshold for EOL capacity	
$\eta_{batt,i}$	lifetime of battery i for optimal operation conditions	days
η^t	lifetime of charging station of type t	days
θ_{cycle}	number of seconds in a bus cycle (60×60)	sec
θ_{day}	number of seconds in a day ($24 \times 60 \times 60$)	sec
θ_{year}	number of seconds in a year ($365 \times 24 \times 60 \times 60$)	sec
κ_i	capacity of battery configuration i	kWh
λ_{deg}	weight of battery life objective in weighted sum method	
λ_{inv}	weight of investment costs objective in weighted sum method	
μ_s	energy consumption between stops s and $s+1$	kWh
ν_s	the required energy to reach the depot from stop s	kWh
π_{depot}	minimum power required to fully recharge battery at depot	kW
π_s^t	maximum power for station type t at stop s	kW
ρ	number of bus cycles each bus performs per day	
τ_s	traveling time between stops s and $s+1$	sec
τ_{depot}	travel time between depot and stop 1 or A	sec
ϕ_s^t	maximum charged energy by station of type t at stop s	kWh
ω	upper bound on the chargeable SOC	
A	number of stops in the model	
N	number of stops in one bus cycle	
	Degradation parameters	
a	parameter for temperature vs. lifetime function	
b	parameter for temperature vs. lifetime function	
d	parameter for cycle lifetime dependent on DOD	

f	parameter for cycle lifetime dependent on DOD	
h	slope of linear SOC-degradation formula	
l	intercept of linear SOC-degradation formula	
m	slope of linear DOD-degradation formula	
n	intercept of linear DOD-degradation formula	
R_{th}	thermal resistance of the battery	$\Omega/°C$
T_{amb}	ambient temperature	$°C$
	Energy consumption parameters	
$\hat{\eta}$	Powertrain efficiency	
ρ_{air}	Air density	kg/m^3
c_d	Aerodynamic drag coefficient	
c_r	Rolling resistance coefficient	
g	Gravitational acceleration	m/s^2
m_v	Vehicle mass	kg
r_a	Acceleration rate	m/s^2
r_d	Deceleration rate	m/s^2
v	Average velocity	m/s
A_f	Frontal area	m^2
	VARIABLES	
b_i	choice of battery size installed in every bus	$\in \mathbb{B}$
e_{cycle}	used energy during one cycle	$\in \mathbb{R}_{\geq 0}$
$h_{dwell,s}$	the area under the graph of SOC during dwell time at stop s	$\in \mathbb{R}_{\geq 0}$
$h_{travel,s}$	the area under the graph of SOC during travel from s to $s+1$	$\in \mathbb{R}_{\geq 0}$
v	minimum energy level reached on a day	$\in \mathbb{R}_{\geq 0}$
w_s	energy in battery when leaving stop s	$\in \mathbb{R}_{\geq 0}$
x_s^t	charging station of type t is build at stop s	$\in \mathbb{B}$
x_d^t	charging station of type t is build in both directions at stop d	$\in \mathbb{B}$
y_s	charged energy at stop s	$\in \mathbb{R}_{\geq 0}$
z_s	energy in battery when arriving at stop s	$\in \mathbb{R}_{\geq 0}$
DOD_i	depth of discharge for battery size i	$\in \mathbb{R}_{\geq 0}$
SOC_i	average state of charge for battery size i	$\in \mathbb{R}_{\geq 0}$
	MODELS	
$A.x$	model with weighted sum method for MOP optimization	$x = 1, 2, 3$
$B.x$	model with ε-constraint method for MOP optimization	$x = 1, 2, 3$
$O.x$	model without battery degradation	$x = 1, 2, 3$
$X.1$	buses have same charge profile for every bus cycle, starting and ending at the same energy level	$X = A, B$
$X.2$	buses have same charge profile for every bus cycle, possible energy depletion	$X = A, B$
$X.3$	buses have different charge profiles for every bus cycle	$X = A, B$

Chapter 1

Introduction

1.1 Introduction to the Topic

Sustainable and environmentally responsible investments have been of growing interest over the past decades. As knowledge of the impact of consumer behavior on global warming and the environment develops, citizens and companies alike are changing their attitude towards their environmental engagement. Change towards more environment-friendly behavior is stimulated by the right policies and policy-makers are aware of this responsibility. In December 2015, 174 countries signed the Paris climate agreement that aims at holding global warming at a maximum of 2 °C. Since greenhouse gasses (GHGs) have a major impact on climate change via the greenhouse effect, the governments involved have promised to build their policies thus to reduce GHG emissions, focusing on CO_2 emissions (Rogelj et al., 2016).

According to data of 2013 an estimated 74% of worldwide GHG emissions can be attributed to the energy sector, of which 21% is due to the transportation industry (World Resources Institute, 2013). A key and viable approach to reducing GHG emissions of the transportation sector is replacing internal combustion engines of transportation vehicles by alternative traction motors. In line with this insight, governments are interested in replacing the conventional internal combustion engine buses (CBs) in urban public transport by electric buses (EBs). Using renewable energy forces, such as solar, wind, geo-thermal etc., to generate the electricity is most effective, but even electric cars recharged from coal-powered generators cut CO_2 emission roughly in half (J. Chen et al., 2013). The technology of fuel cells is very promising as well with regard to emissions reduction, efficiency, operability and maintenance. However, a recent study shows that fuel cell buses are roughly twice as expensive as EBs and therefore the current focus for the public transport sector lies primarily in transition to EBs (Lajunen, 2014).

Generally, there are two options, EBs that draw electricity from overhead catenary wires or EBs with an on-board energy storage system (ESS). The latter is commonly preferred, since the catenary-powered EBs require more maintenance, induce visual pollution with the wires and are inflexible regarding re-routing in case of disturbances. In the past, the energy storage has been a technological barrier for employment of EBs for public transport, but with the development of lithium-ion (Li-ion) batteries an adequate performance is achieved in terms of power and energy capacity (Scrosati and Garche, 2010; Burke and Miller, 2011).

The Li-ion batteries in EBs are capable of *fast-charging*, employing charging powers of hundreds of kilowatts. This enables batteries to be recharged at bus stops while passengers board and disembark, decreasing required battery sizes and increasing energy efficiency. However, it also demands for a more extensive charging infrastructure in order to guarantee network-wide coverage, leading to an increase in investment costs and making it the main cost driver (L. Wang et al., 2015).

Approximating the lifetime of the batteries on board is crucial for cost optimization but also quite complicated. Battery manufacturers typically define the lifetime performance in deep discharge-charge cycles in constant and low current rate conditions which may not correspond well to the real operating conditions (Lajunen, 2014). Existing network design models assume the battery lifetime as a predefined constant, whilst charging patterns, defined by the solution of said models, directly affect battery ageing and thus its lifetime. Therefore, the aim of this research is to integrate the lifetime approximation in a charging network design model to improve the design of an electric urban transportation network.

This Chapter further includes the motivation and relevance of this research and a review of the literature relevant to the subject. In Chapter 2 the framework of the problem is described, including some technological background information on batteries and a list of assumptions that define the problem. The methodology is discussed in Chapter 3, including the battery degradation modeling as well as methods for multi-objective optimization modeling and the formulation of the resulting network design model. In order to obtain results the model is tested on data based on a bus line in Rotterdam. The methods for finding the required data are described in Chapter 4. Various results are discussed in Chapter 5 and some concluding remarks can be found in Chapter 6.

1.1.1 Motivation and relevance of research

Electrification of bus networks is an interesting option for improving environmental sustainability. However, the research in optimization of these networks is rather scarce. In order to promote electrification of current bus networks, an optimal network design is essential. With this research, I aim to integrate battery degradation in a Mixed Integer Linear Programming (MILP) model for optimal network design for EBs with on-board ESS.

In previous research, both charging infrastructure models for electric transportation networks and charging policies with the goal of retaining battery degradation have been developed separately (i.a. Hoke et al., 2011; J. Chen et al., 2013; Wehres et al., 2016; Pelletier et al., 2017). Although there is a trade-off between the battery lifetime, battery size and the charging infrastructure, a network design model with an integrated battery degradation model has not yet been developed. This gap is filled with this research, enabling the design of a smarter electric urban transport network. Since the trade-off between charging infrastructure and battery lifetime is involved in the solutions, the total cost of ownership (TCO) estimation is improved. An accurate TCO estimation is of great importance to public transportation companies and local and national governments. This model can serve as a tool to make an informed decision about electrifying the public transport network.

1.2 Literature Review

The literature regarding urban electric buses powered by on-board batteries that is relevant to this research is described per topic in this section.

1.2.1 Technical feasibility of bus network electrification

Before designing a charging infrastructure for EBs with on-board ESS it is important to know whether the technology is sufficient to operate on a public transport network and what the impact on the electrical grid is. One example of such research is

the analysis of the bus network in Muenster, Germany (Rogge, Wollny, and Sauer, 2015). The feasibility of electrifying the bus network is assessed through simulation. Energy consumptions for separate trips were obtained, trips were then combined in individual vehicle schedules and the resulting power profiles were derived for every charging station and the entire network. The required battery capacity for each bus route is calculated under the various charging power conditions. Sufficient capacity could be achieved for almost all routes with maximum charging power at 46% of the charging opportunities. This can be quite strenuous for the electric grid, but the authors argue that this can be smoothened with an intelligent control algorithm that takes future charging possibilities in account. Also, the usual energy density of batteries is likely to increase in the near future, leading to higher capacity on-board ESS and lower demand for charging. This analysis proves the technical feasibility of electrification of a large part of the bus network in Muenster without altering the routes and schedule. Although this is very case-specific, it exemplifies the conditions under which electrification of a bus network is realizable.

The strain on the electrical grid can be improved by smart charging policies (Lyon et al., 2012). Electric vehicle charging can significantly increase demand and strain the capacity of existent electricity grids during peak periods. Charging policies can help to shave peak demands by allocating charging opportunities. If fast charging stations are employed with ESS as well, the peaks in electricity demand can be smoothened further and the strain on the grid and even electricity purchase cost can be reduced. This is shown in an analysis of an existing EB network in China (Ding, Z. Hu, and Song, 2015). Installing ESSs in the charging stations and smoothing the demand peaks decreased the annual electricity costs with 36% in this case, implying a decrease in the strain on the grid. These results support the expectation of technological feasibility.

1.2.2 Economic feasibility of bus network electrification

Next to the technical feasibility, the economic side of transition to an electrical bus fleet is of great importance. Even though the capital costs of electric city buses are high, they are generally more durable than CBs, decreasing maintenance and replacement costs, and the lower energy consumption significantly reduces the operating costs compared to conventional buses. An electric bus network therefore has the potential to outperform an CB-operated network not only in CO_2 emissions, but also in lifetime costs. The on-board battery, including its management system, is the most important factor affecting the lifetime and costs of EBs, but costs are expected to significantly drop in the future (Lodi, Manzoni, and Crugnola, 2010; Santini, Gallagher, and Nelson, 2010; Wood, Alexander, and Bradley, 2011). Also the maintenance costs for an EB could be considerably lower than for a CB (Feng and Figliozzi, 2013). On the other hand, EBs require charging equipment and infrastructure supporting their operation, which increase initial costs. However, this kind of infrastructure is much more durable than the EBs, and the eventual cost impact on the life cycle cost of the bus fleet operation is not that significant (Lajunen, 2014).

Exact cost analysis of EBs is difficult, since its technology is fairly new and mass production has not yet been initiated (Van Vliet et al., 2010). However, approximations of the costs involved can be obtained through simple analyses. Price forecasts can be estimated based on technological learning rate, but research showed that technological development of battery electric vehicles is complicated to estimate, since the production process is not as mature as with conventional cars (Weiss et al., 2012). Some case studies can be found that apply various methods to approximate the costs

involved. An analysis of the bus network in Minneapolis, Minnesota assessed the capital and operating costs for varying configurations of charging stations and battery sizes (L. Wang et al., 2015). No configuration could beat the CBs in terms of costs, but for some bus lines the costs of EBs and CBs were similar. It is important to note that this analysis did not involve cost-optimization. Another case study for six different routes showed that there are likely scenarios in which the life cycle costs of EBs beat those of CBs, such as when battery costs decrease and fuel costs increase (Lajunen, 2014).

In summary, initial costs of a transportation network operated by EBs are relatively high compared to conventional transportation systems, but are expected to drop. Moreover, EBs generally have a longer lifetime and operation and maintenance costs are significantly lower, making it a more durable investment. Therefore electrification of a bus network can be a profitable investment when implementation is optimized.

1.2.3 Charging network design

The difference between network design for regular buses and for EBs is that for a regular bus network the social benefit is optimized with respect to budget or rolling stock constraints whereas for an EB network the design resembles a facility location problem with added complexity of hierarchical decisions for the battery size and charging infrastructure. Optimization models for the design of a charging network for electric vehicles for individual use, the so-called electric vehicle charging station placement problem (EVCSPP), are well represented in literature, but specifically for public transport the literature is rather scarce. Since in public transport buses travel along predefined paths, another, more specific approach is necessary.

Two mathematical optimization models for a single electrical bus line can be found in existing literature (J. Chen et al., 2013; Wehres et al., 2016). Both optimize placement of the charging stations and battery configuration simultaneously, but the approaches differ slightly in the assumptions that frame the problem. Different constraints for the decision on configuring on-board batteries and charging station types were used, employing binary or continuous variables. In one paper a method for incorporating uncertainty in energy consumption is proposed by means of *budget of uncertainty* (Wehres et al., 2016).

Battery lifetime is assumed as given in both papers. However, a suggestion was made to add a battery temperature constraint, restricting the temperature of the battery and securing it's lifespan (J. Chen et al., 2013). These models serve as basis for the network design model that is presented in this thesis, incorporating battery degradation to optimize the investment decision with dynamic battery lifespans.

Chapter 2

Problem Framework

In this Chapter some background information regarding battery technology is provided in Section 2.1. The problem under consideration is described in detail in Section 2.2. Together, this information will outline the framework in which the model is developed.

2.1 Technological Background

Since the goal of this research is to incorporate battery behavior and degradation in a charging station placement model, some technological background information regarding these subjects is provided here.

2.1.1 Battery behavior

In order to evaluate battery degradation, it is important to model the behavior of a battery as accurate as possible. Batteries are usually modelled as an equivalent electrical circuit, as this provides a clear insight of the processes involved. Such a circuit model, depicted in Figure 2.1, consists of an open-circuit voltage source ($V_{OC}(SOC(t))$) connected with an internal battery resistance $R(SOC(t))$ in series. Here t indicates time and $SOC(t)$ is the state of charge at time t, i.e., the relative energy level in the battery. The open-circuit voltage of the battery corresponds to when there is no current flowing through the battery, i.e., no external demand or input of electricity is connected to the battery. The open-circuit voltage is increasing in SOC, as can be seen in Figure 2.2.

The actual instantaneous voltage, or terminal voltage, of the battery itself ($V_{term}(t)$) differs from the open-circuit voltage. When the battery is charged or discharged the

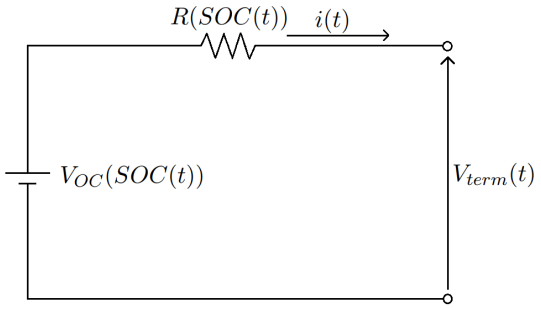

FIGURE 2.1: *Simple battery equivalent circuit model, portrayed in state of discharging*

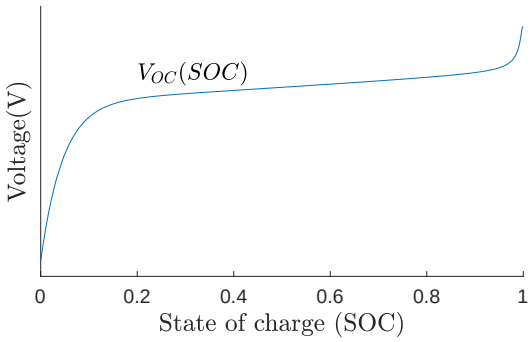

FIGURE 2.2: *The relation between state of charge and open-circuit voltage within a battery, obtained from (Pelletier et al., 2017)*

terminal voltage is respectively superior or inferior to the open-circuit voltage because then current flows into or out of the battery. The open-circuit voltage and internal resistance are directly mappable by SOC and can be used to determine $V_{term}(t)$ (Marra et al., 2012; Pelletier et al., 2017). The parameters of the battery model can be extracted from a discharge curve, by making some simplifying assumptions. It is assumed that the internal resistance R is constant, temperature has no influence on the parameters and parameters are equal for charging and discharging. For a more extensive explanation of the method for extracting the parameters the reader is referred to Tremblay, Dessaint, and Dekkiche (2007). The model can be described by the following equation, $i(t)$ denotes the current at time t, and is positive during discharging and negative during charging.

$$V_{term}(t) = V_{OC}(SOC(t)) - R \cdot i(t) \tag{2.1}$$

The resulting model describes an increase in terminal voltage when SOC is higher. This model is fairly simple but sufficient for this research. Many different methods for equivalent circuit battery modeling can be found in literature, varying in complexity and accuracy (e.g. M. Chen and Rincon-Mora, 2006; Zheng, Qi, and Du, 2009; Larminie and Lowry, 2012; Rahmoun and Biechl, 2012; Liu, 2013).

The equivalent electric circuit model equips us with a relation between voltage, current and SOC. This enables the modeling of battery behavior during charging and discharging. Generally one of two different charging modes is applied, constant current-constant voltage (CC-CV) or constant power-constant voltage (CP-CV) (Pelletier et al., 2017). Both are explained here.

In the CC-CV scheme, the battery is first charged with constant current, the CC-phase. The rate of change in SOC can be found with

$$\frac{d}{dt}SOC(t) = -\frac{i(t)}{Q},$$

with Q denoting the maximum capacity (Moura et al., 2011). The rate of change is proportional to the current, so the SOC increases linearly in the CC-phase. As SOC increases, terminal voltage of the battery increases. In order to avoid overcharging, the terminal voltage can not exceed a specific maximum value. As the terminal voltage reaches this value, the charging continues in the CV-phase, where voltage is held constant. The open-circuit voltage will continue to increase as SOC increases and to ensure terminal voltage remains constant, the current has to decrease exponentially, incurring an concavely increasing SOC.

In the CP-CV scheme, the power is held constant in the first phase. The relation between power, voltage and current is described with

$$P_{charge}(t) = V_{term}(t) \cdot i(t),$$

with $P_{charge}(t)$ denoting the charging power. Since the open-circuit voltage increases as SOC increases, consequently the terminal voltage increases as SOC increases and the current has to decrease to maintain constant power. As the rate of change in SOC is proportional to the current, SOC will increase with decreasing rate. When the terminal voltage reaches its maximum, the voltage is held constant and CV-phase is entered. Throughout both charging schemes, the battery's SOC does not increase in a linear fashion (Pelletier et al., 2017).

An explanation on battery behavior during discharging is omitted, since it is of no further interest for this research.

2.1.2 Battery degradation

Before explaining the aspects of battery degradation, first some terminology is introduced. We distinguish bus cycles and battery cycles. A bus cycle is defined as one round trip of a bus, i.e. the sequence of stops a bus visits, starting and ending at the same terminal after which the same sequence of visits is repeated. A battery cycle is the time between two consecutive full recharges of a battery. Both are visualized in Figure 2.3. One bus cycle could encompass several battery cycles, if an on-board battery is at least once fully recharged on the route as in Figure 2.3, or vice versa, if the on-board battery is only fully recharged after several round trips of a bus. An important battery level measure for degradation is depth of discharge (DOD). DOD is defined as the largest difference in SOC during a day of operation, visualized in Figure 2.3 as well.

Batteries are subject to various internal and external factors that influence the lifetime of a battery. Batteries are in essence a way to store electrical energy as chemical energy and retrieve the electrical energy on a desired moment in time. This process is dependent on chemical reactions, so-called redox reactions, but over time the chemical components involved deteriorate and subsidiary products of the reaction accumulate at the reaction surface, decreasing the efficiency of the reaction and capacity of the battery. When the capacity is decreased to an end-of-life (EOL) level

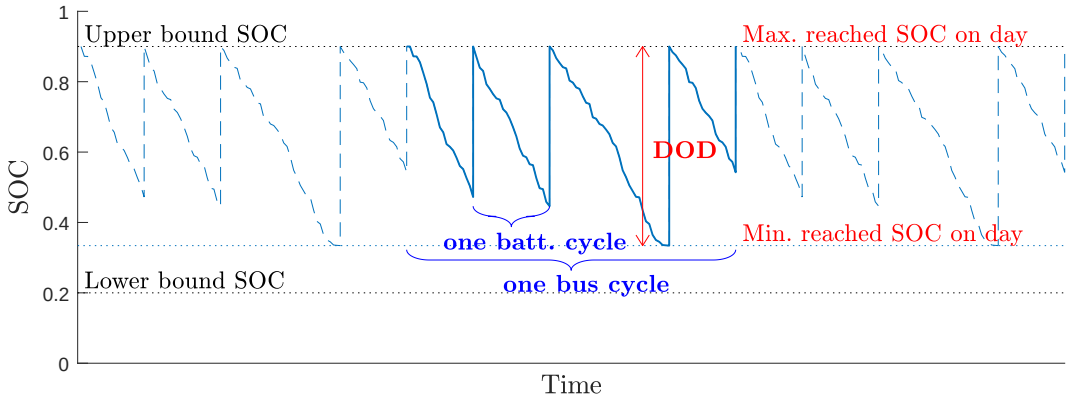

FIGURE 2.3: *An example of the development of the SOC in a bus battery, three consecutive bus cycles are depicted, the difference between a bus and a battery (batt.) cycle is emphasized as well as the definition of DOD. In this example, one bus cycle encompasses four different battery cycles.*

the battery is insufficient for further use and must be replaced. This is due to natural processes that happen over time, but external factors enhance these effects, such as temperature, SOC, DOD, cycling rate and overcharging and -discharging (Ecker et al., 2014; Pelletier et al., 2017). Overcharging and overdischarging happens when the terminal voltage within the battery exceeds predefined bounds. Since the effects of over(dis)charging on the battery aging are substantial and this is easily controllable by limiting the usable voltage, in most literature the usable voltage is reasonably assumed to be restricted and, consequently, overcharging and overdischarging are assumed to never occur.

It is important to distinguish cycle lifetime from calendar lifetime in terms of degradation. Cycle lifetime is a way to express performance, i.e., how many battery cycles will a battery be able to complete before it reaches its EOL capacity, rather than calendar lifetime, which is an expression of time until the battery reaches its EOL capacity. Deterioration occurring during charging and discharging generally corresponds to cycle aging and deterioration occurring during storage corresponds to calendar aging. Cycle aging is affected by e.g. DOD and temperature fluctuations due to (dis)charging, calendar aging by e.g. the SOC-level and the temperature a battery is stored at. For this research we are interested in cycle aging that can be attributed to the operation decisions.

Various battery degradation models have been described in existing literature (e.g. Peterson, Apt, and Whitacre, 2010; J. Wang et al., 2011; Hoke et al., 2011; Xu, 2013; Omar et al., 2014; Sekyung Han, Soohee Han, and Aki, 2014; Sarasketa-Zabala et al., 2015). The definite choice of modeling battery degradation is explained in Chapter 3.

2.2 Problem Description

The considered problem involves placement of charging stations along a single bus line. Charging network design models found in literature form the basis for the model presented in this thesis, and a similar problem framework is used (J. Chen et al., 2013; Wehres et al., 2016). The EB-industry demands a more accurate TCO estimation and minimization to increase its attractiveness for investment and with it its growth and development. To make investing in an EB transport system more appealing not only the initial investment costs should be minimized, but also the durability of the investment should be maximized. Therefore the problem has two objectives, minimizing the investment costs and simultaneously maximizing the battery lifetime.

For simplification reasons and the completeness of the problem framework, the problem is embedded in a number of assumptions. The setting and some of the assumptions of the problem as are applied in the model are explained here and all

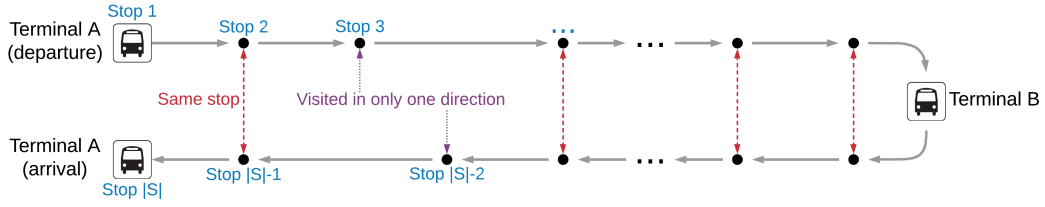

FIGURE 2.4: *Example of interpretation of regular bus line as circle route, same stops on back and forth direction are connected with dashed arrows*

of the assumptions are listed at the end of the Section for a clear overview of the framework.

The bus line is assumed to be a circle route, starting and ending at the same terminal stop. A regular bus line route (with different origin and destination) can also be interpreted as a circle route by considering both the back and forth direction. With this approach all stops between the two terminal stops are visited twice, with potential exceptions for stops that are only visited in one of the directions. In Figure 2.4 this is visualized.

The only difference of a terminal compared to a regular bus stop from a modeling perspective are the length of the dwell time, which is considerably longer at terminal stations, and the fact that at a terminal station a charging facility is *always* installed. Modeling charging station placement for a regular bus line is identical to a circle route, if installing charging stations for both directions at the same stop is not beneficial with regard to costs compared to installing them at different stops. In this research, however, the possibility of saving expenses by installing charging stations at both directions of a stop compared to installing them at two different stops is incorporated in the model.

Additionally, the setting of the bus line involves a depot at which the buses reside during the night. Here the buses have the opportunity to fully recharge, thus up to an SOC level of 100%. During operation buses can only attend the charging stations installed along the bus line, which are all fast charging stations. These are unfit for a full recharge up to 100% SOC, due to technical limitations of fast charging. The last 10% of SOC is assumed to be unfit for fast charging and as a consequence on-board batteries can only be recharged up to a SOC of 90% during operation. Although the charging stations at terminal stops might technologically be able to recharge the batteries up to 100%, for ease of modeling the upper bound of SOC for recharging is assumed to be 90% as well.

The end-of-life capacity of a battery is assumed to be 80% of its original capacity. Therefore the first 20% of the battery capacity cannot be used for operation. This means that the SOC during operation will always be bounded below by 20% and above by 90%, in line with generally used cut-off values (Wehres et al., 2016). Only at the depot, after operation has ended, is a battery able to be recharged fully to 100%.

Although the energy required for moving an electric bus is heavily dependent on uncertain, external factors such as passenger load, weather, traffic congestion, auxiliary systems, it is assumed to be known and fixed. The uncertainties are handled as deterministic, stochastically modeling the uncertainties is left out of the scope of this analysis. Because energy-consumption along the route is assumed to be fixed, an operation day can be described completely by a single bus cycle.

2.2.1 List of assumptions

Charging stations

- Two types of charging station are considered for installment along the route: 'fast-feeding station' (FFS), fast-charging at high power, with integrated ESS and 'standard feeding station' (SFS), without integrated ESS, also fast-charging but at lower power and lower capacity than FFS.
- Terminal stops are employed with a third type of charging stations. These are referred to as terminal feeding stations (TFS) and charge at even slower rate.

- Charging occurs at constant power at all charging stations, i.e., only the CP-phase of CP-CV charging policy is performed. Although this involves a non-linear pattern, it is assumed to be linear.
- The charging power is limited according to the type of station and is assumed to be as low as possible, utilizing the available dwell time fully for recharge.
- Coupling and decoupling of the bus with the charger takes negligible amount of time.
- A charging station is always able to recharge the built-in ES between two consecutive buses.

Fleet and on-board battery

- Only one type of bus is considered.
- The on-board ESS is chosen from a predefined set of battery configurations. All buses in the fleet are employed with the same battery size, resulting in a homogeneous fleet.
- The last 10% of the battery capacity is assumed not to be suitable for fast-charging. For ease of modeling this bound for charging is imposed at all charging stations on the route, implying that during an operation day the SOC never exceeds 90%.
- Overnight, on-board batteries are recharged up to 100% at the depot, implying that the battery level starts operation at a SOC of 100% minus the required energy to travel from the depot to the starting terminal stop.
- The end-of-life of a battery is when capacity is reduced to 80% of initial value, making the first 20% of the battery capacity unusable.
- Only degradation due to operation is relevant. The degradation effect to cycle life is isolated as much as possible by normalizing the calendar aging.

Bus line and daily operation

- The line consists of two terminal stations between which the buses alternate, and is treated as a circle route as in Figure 2.4.
- All stops in the route are treated as separate, but a reduced tariff for installing charging stations in both directions of the same stop can be applied. In total there are A stops in the model.
- The energy consumption for traveling is assumed to be known and fixed, uncertainty is left out of the scope of this research
- All operation days are assumed to be equal in charging decision and energy consumption.
- Buses start their operation day at the depot, travel to the first terminal stop, then operate the bus line for a number of bus cycles, after which they return from the ending terminal to the depot.
- Discharging is assumed to happen linearly with respect to SOC.
- A bus should be able to return to the depot from any point in the route.
- The initial battery level and its development during a bus cycle is equivalent for all bus cycles. Only the trips from and to the depot at the start and end of the day are modeled separately.

Chapter 3

Methodology

In this Chapter the charging station placement model is presented according to the framework described in Chapter 2. The model described here is mainly based on the charging station placement model presented in the research of Wehres et al. (2016). In Section 3.1 the concept of multi-objective optimization is explained. The used notation for the model is described in Section 3.2 and in Section 3.3 battery degradation modeling is described. In Sections 3.4 and 3.5 the MILP is presented and in Section 3.6 two extensions to the basic model are proposed.

3.1 Multi-Objective Optimization

The problem has two different objectives: minimizing capital costs and maximizing battery life. In order to incorporate both in a model, they must be expressed in a comparable manner. Battery degradation is therefore expressed in *relative loss in lifetime*, which is described in Section 3.3.

The two objectives are conflicting as improving one can have a negative impact on the other. E.g. a solution with a few fast charging stations installed on the line would have low investment costs, but can also diminish battery lifetime due to large DODs. A mathematical problem with multiple conflicting objectives is referred to as MOP (Multicriteria Optimization Problem) of the Pareto class (Ehrgott, 2006). An MOP can be denoted as follows.

$$\min_{x \in \mathcal{X}} (f_1(x), \ldots, f_p(x)) \tag{3.1}$$

Here $\mathcal{X}$ denotes the feasible space. Various methods for dealing with conflicting objectives have been developed in the field of mathematical optimization. For this research two of those methods are applied to design two different models, and the results of both will be assessed and compared.

One of the methods is the weighted sum method. This involves an MOP being solved by solving a single objective function problem. The involved objectives are each weighed by a factor λ_k and aggregated in a sum. The weighted sum method and the resulting model will be described in Section 3.4.

The other method is the ε-constraint method, which also reduces an MOP to a single objective optimization problem. One of the objectives is optimized and the rest of the objectives is restricted by a preset bound and incorporated in the constraints. Here the battery lifetime objective will be incorporated as ε-constraint. The ε-constraint method and the resulting model will be described in Section 3.5.

Both of these models optimize the charging network under the assumption that a full day of operation can be described by a single cycle. In Section 3.6 some extensions to the model are proposed for relaxing this assumption and allowing a

more complex operation optimization, potentially more adequate in retaining battery degradation.

Since the charging stations are of the fast-charging type, they require an ESS as well, which is required to be fully recharged in between consecutive buses that visit the charging station. The charging decision of an ESS in a FFS would likewise have an impact on its lifetime. However, the main focus of this thesis is the lifetime of the on-board batteries. Therefore this charging behavior is irrelevant for our research and for simplification reasons the time between consecutive buses, available for recharging the FFS, is preconditioned to always be large enough for a full recharge.

3.2 Notation

The basis for the notation for the sets, parameters and variables used in the design of the models is enlisted here, followed by a mathematical representation of the problem described in Chapter 2.

Sets

Station types: $t \in T = \{FFS, SFS, TFS\}$

Stops: $s \in S = \{1, \ldots, A\}$

Unique stops: $d \in D$

Back-forth stop pairs: $s \in S^d \subset S$

Terminals: $s \in S^{TFS} \subset S, \ \{1, A\} \subseteq S^{TFS}$

Battery sizes: $i \in I$

Parameters

β	number of buses in the fleet operated on the route
γ_{batt}	marginal cost of a battery (€/kWh)
κ_i	capacity of battery configuration i (kWh)
$\Gamma_{batt,i}$	cost of battery configuration i, $\gamma_{batt} \cdot \kappa_i$ (€)
Γ_s^t	cost of installing charging station of type t at stop s (€)
α_d^t	savings of both way installing charging station of type t at stop d, $\alpha_d^t \leq 0$ (€)
ζ	lower bound on the usable SOC, the threshold for EOL capacity
ω	upper bound on the SOC suited for fast-charging technology
ρ	number of bus cycles each bus performs per day
ν_s	the required energy to reach the depot from stop s (kWh)
μ_s	energy consumption between stops s and $s+1$ (kWh)
τ_s	traveling time between stops s and $s+1$ (s)
τ_{depot}	traveling time between depot and stop 1 or stop A (s)
δ_s	available dwell time at stop s (s)
δ_{depot}	charging time at depot for full recharge for on-board battery (s)
π_s^t	maximum power applied by station of type t at stop s (kW)
π_{depot}	minimum power required to fully recharge on-board battery (kW)

ϕ_s^t maximum charged energy by station of type t at stop s (kWh)

$\eta_{batt,i}$ lifetime of battery size i in days, under optimal conditions

η^t lifetime of charging station of type t in days

θ_{day} number of seconds in a day, equal to $24 \times 60 \times 60 = 86,400s$

θ_{year} number of seconds in a year, equal to $365 \times 24 \times 60 \times 60 = 31,536,000s$

Variables

b_i binary variable, indicating the choice of battery size installed in every bus

x_s^t binary variable, indicating if a charging station of type t is build at stop s

x_d^t binary variable, indicating if a charging station of type t is build in both directions at stop d

y_s charged energy at stop s

z_s energy in battery when arriving at stop s

w_s energy in battery when leaving stop s

v minimum energy level reached on a day

$h_{dwell,s}$ aux. variable for average SOC level during dwell time at stop s

$h_{travel,s}$ aux. variable for average SOC level during travel between stop s and $s+1$

The bus line can be represented by a graph $\mathscr{G} = (\mathscr{V}, \mathscr{E})$ with for every stop on the line a node, two nodes for the terminal station (node 1 and A, start and end of the line resp.) and one node for the depot, denoted by 0. The set of nodes is thus $\mathscr{V} = S \cup \{0\}$. All consecutive stops are connected by an edge which has a length of the corresponding energy consumption μ_s. The same holds for the traveling time. Furthermore, every stop $s \in S$ is connected with the depot with an edge of length ν_s.

3.3 Degradation Functions

In Chapter 2 it was explained that several factors contribute to the battery degradation. In this research battery degradation is defined as the sum of degradation attributable to single factors, splitting up the degradation for each factor involved. The most significant factors that influence capacity degradation during a daily battery cycle are DOD, temperature and open-circuit voltage, which is mappable by SOC (Hoke et al., 2011). The degradation due to these factors can be expressed linearly and therefore these are suitable for this research. In order to combine the objectives of minimizing lifetime costs and maximizing battery lifetime, battery degradation is expressed as relative lifetime loss, $\frac{\Delta L}{L}$. All degradation functions adopted for this model are based on the idea of determining the relative lifetime loss incurred by a daily battery cycle for each factor separately, thus finding an expression for the contribution to battery degradation (Hoke et al., 2011). Here ΔL describes the lifetime *degradation* that can be attributed to the battery cycle that is evaluated and L is the total battery lifetime if the evaluated battery cycle is repeated until EOL-capacity is reached. For isolating degradation factors a battery degradation tool of the National Renewable Energy Laboratory (NREL) is employed (Smith et al., 2010).

The approach of expressing battery degradation in relative lifetime loss is suitable for both MOP-methods. For the weighted sum method it is necessary to express both objectives in a similar unit, and relative lifetime loss is easily transformed to

degradation costs by multiplication with the battery costs. The relative lifetime loss is also easily transformed to a total lifetime in operation days and vice versa, since they are inversely related. For the ε-constraint method a bound can be chosen for a minimum desired lifetime in operation days, which can be transformed to a maximum allowed relative lifetime loss per day. The degradation functions have the following form, superscript λ for the weighted sum method, and superscript ε for the ε-constraint method.

$$g_{deg}^{\lambda,X} = \Gamma_{batt} \cdot \frac{\Delta L_X}{L} \qquad g_{deg}^{\varepsilon,X} = \frac{\Delta L_X}{L} \tag{3.2}$$

Three factors that have impact on the lifetime degradation are identified: DOD, SOC and temperature. The superscript X indicates the degradation factor ('*DOD*', '*SOC*' or '*Temp*'). In order to fit the linearity of the model, the lifetime loss should be expressed linearly for the various factors and the rate of degradation should be independent of time and the amount of capacity left in the battery. In reality this might not exactly be the case, but it is assumed that the impact on the rate of degradation is negligible and the average rate of degradation is assumed to be sufficient. An example of the decline in battery capacity is depicted in Figure 3.1. The degradation functions are discussed per factor in the rest of this Section.

3.3.1 DOD-related degradation

First we discuss the degradation related to DOD. The corresponding degradation function is based on a relation between the battery lifetime in battery cycles and the DOD in all those battery cycles in its lifetime. Effects of cycle-*frequency* are not captured with this function, but those are captured with the degradation function related to temperature. The relation between DOD and battery lifetime in cycles N is described by the following equation (Hoke et al., 2011).

$$N(DOD) = \left(\frac{DOD}{d}\right)^f \tag{3.3}$$

Here it was assumed that n battery cycles at a given DOD have the same effect on the amount of life cycles as n battery cycles with an *average* DOD_{avg} over all n battery cycles equal to that DOD. It is noted that the degree of validity of this approximation

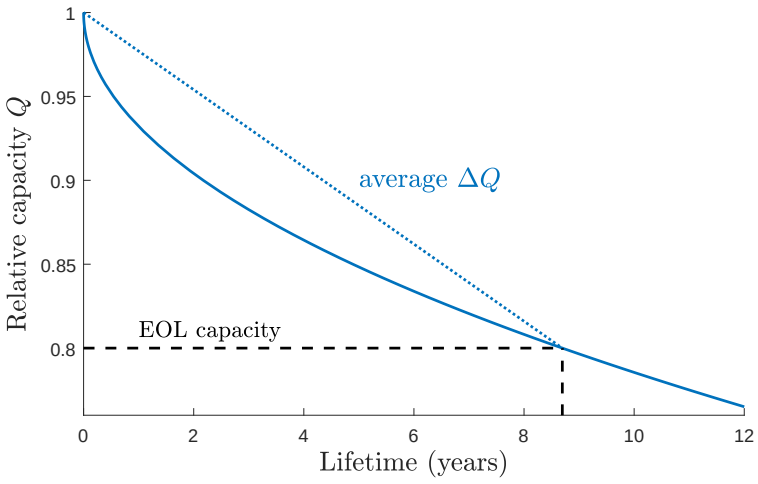

FIGURE 3.1: *An example of the decline in battery capacity over time*

is difficult to assess from the available data. To determine the degradation costs, the concept of *energy throughput* is employed (Marano et al., 2009). Lifetime energy throughput (E_{TL}) for a given average DOD_{avg} over all battery cycles in a battery lifetime is defined as

$$E_{TL} = N(DOD_{avg}) \cdot DOD_{avg} \cdot \kappa_{batt}.$$

A battery cycle j with DOD of DOD_j changes the average DOD_{avg} slightly to $DOD_{avg,j}$ and also uses up an energy throughput of $DOD_j \cdot \kappa_{batt}$. The altered energy throughput due to the battery cycle is then

$$E_{T,used} = N(DOD_{avg,j}) \cdot DOD_{avg,j} \cdot \kappa_{batt} + DOD_j \cdot \kappa_{batt}.$$

This used energy throughput is compared with a baseline energy throughput $E_{T,base}$, derived from a baseline DOD of DOD_{base} (Hoke et al., 2011). It is, however, unclear from the literature how the baseline DOD can be derived. We assumed here that it is equal to the lifetime energy throughput, a reasonable assumption, regarding the fact that we want to assess the relative loss in lifetime. The degradation is expressed as relative loss in energy throughput due to the daily battery cycle compared to the base line energy throughput as follows.

$$\frac{\Delta L_{DOD}}{L} = \frac{E_{T,used} - E_{TL}}{E_{TL}} \tag{3.4}$$

A similar approach uses a slightly different expression (Barco et al., 2017). The relative lifetime loss due to DOD is described by the ratio between energy throughput of one battery cycle and the total energy throughput throughout a battery lifetime. Energy throughput of one battery cycle is calculated as

$$E_{T,cycle} = DOD_j \cdot \kappa_{batt}$$

and energy throughput of battery lifetime E_{TL} similar as above, using the same formula (3.3) to calculate battery lifetime in cycles. Then the degradation is expressed as follows.

$$\frac{\Delta L_{DOD}}{L} = \frac{E_{T,cycle}}{E_{TL}} \tag{3.5}$$

This seems somewhat more intuitive, since this results in $\frac{\Delta L}{L}$ lines that go through the origin, i.e., if a battery cycle would have a DOD of 0, the relative lifetime loss is also 0, whereas the function (3.4) results in $\frac{\Delta L}{L}$ lines where for a battery cycle of DOD 0, still a relative lifetime loss of larger than 0 would be attributed to it. This indicates that it also accounts for calendar lifetime loss that would occur under storage conditions, which is not of interest in this research.

An immediate issue arises regarding the functions usability in a linear optimization problem, i.e., the non-linear nature of the relation. Therefore we need to find a linear equivalent equation. We can evaluate the degradation functions for various average DODs and find the relation between relative lifetime loss and DOD of a battery cycle for the various average DODs separately. This is visualized in Figure 3.2. These are linear relations, and thus, an option for applying it in the optimization problem would be to choose an average DOD beforehand, apply its corresponding lifetime-loss-function in the optimization and evaluate after solving if the resulting average DOD is close enough to the chosen value. The DOD resulting from the solution would be equal to the average DOD over the lifetime of a battery, since it

is assumed that the charging pattern is equal for all operation days. Choosing an average DOD and optimizing can be done iteratively until an satisfactory result is reached. The degradation function can now be rewritten.

$$\frac{\Delta L_{DOD}}{L} = m \cdot DOD + n \tag{3.6}$$

Here, m denotes the slope of the chosen lifetime-loss-function and n the corresponding intercept (the intercept n is always 0 with the formulation (3.5)).

In Algorithm 1 the pseudocode is described for the iterative process of solving the MILP with the correct parameters for the DOD-degradation. An average DOD (and the corresponding parameters) is assumed before solving the MILP, denoted by $DOD_{ass,z}$. When a solution z is found, the battery degradation due to DOD needs to be adjusted in the solution using the DOD degradation parameters corresponding to the average DOD that belongs to the solution, $DOD_{true,z}$. Depending on the applied MOP-solving method, this can either involve altering the objective value (weighted sum method) or reevaluating the feasibility of the solution (ε-constraint method). As can be seen in Figure 3.2, DOD degradation increases for larger average DOD. When a solution has a lower value for $DOD_{true,z}$ than the predefined average DOD value, the true DOD-degradation will also be lower, and vice versa. After adding the adjusted solution to the set of solutions, a new value for assumed DOD is found with the function $f_{nextDOD}$. Examples of this function are to assume the last $DOD_{true,z}$, to take the average between $DOD_{true,z}$ and $DOD_{ass,z}$ or simply to go over a list of predefined values. Since the found solution depends on the DOD-degradation function corresponding to the assumed DOD value, the new average DOD is compared to all previous values for $DOD_{ass,z}$. If the difference is small, it is likely to find the same solution as before and no other solutions can be found. From the set of found solutions, the (feasible) solution with lowest objective value is chosen as optimal.

Another option that would not require this iterative process of adjusting the parameters to match the solution DOD would be to approximate the curve of the markers in Figure 3.2 linearly. The markers indicate the points where the assumed average DOD aligns with the true value for average DOD. However, this would induce an approximation of an already simplified degradation model, risking a decrease in accuracy.

In this research equation (3.5) is used to describe the relation between a cycle DOD and lifetimeloss. It is preferred over equation (3.4) based on the intuition that it

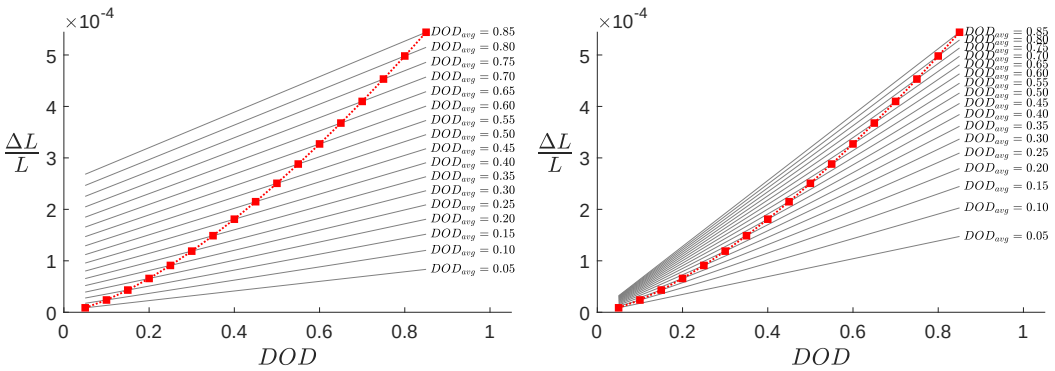

(A) Using equation (3.4)

(B) Using equation (3.5)

FIGURE 3.2: *The relative loss in lifetime due to the DOD of a battery cycle for various average DODs. The red markers indicate where the DOD value corresponds to the average DOD.*

Algorithm 1 Iterative process for DOD-degradation function

Z := set of found optimal solutions
z^* := best solution
$v(z)$:= objective value of solution z
ϑ := threshold value for finding new solutions
DOD_{ass} := current assumed average DOD for $g_{deg}^{\lambda,DOD}$
$DOD_{ass,z}$:= assumed average DOD for finding solution z
$DOD_{true,z}$:= true average DOD of solution z
$f_{nextDOD}$:= function to find next DOD_{ass}
$f_{m,n}(DOD_{avg})$:= function to find param m and n for $g_{deg}^{\lambda,DOD}$

initialize ϑ, DOD_{ass}
initialize $(m,n) \leftarrow f_{m,n}(DOD_{ass})$
while more solutions can be found **do**
    solve MILP
    $z \leftarrow$ solution MILP
    $(m,n) \leftarrow f_{m,n}(DOD_{true,z})$
    adjust z with correct DOD degradation
    add z to Z
    $DOD_{ass} \leftarrow f_{nextDOD}$
    for all $z \in Z$ **do**
        if $|DOD_{ass} - DOD_{ass,z}| < \vartheta$ **then**
            no more solutions can be found
        end if
    end for
    $(m,n) \leftarrow f_{m,n}(DOD_{ass})$
end while
$z^* \leftarrow \underset{z \in Z}{\operatorname{argmin}}\, v(z)$

better represents cycle aging. Four methods are compared for dealing with the non-linearity of DOD-degradation. Three of which employ the iterative algorithm with following functions $f_{nextDOD}$ for finding the assumed DOD for each next iteration i.

(1) $DOD_{ass,i+1} = DOD_{true,i}$ referred to as method '*last*'
(2) $DOD_{ass,i+1} = \frac{1}{2}(DOD_{true,i} + DOD_{ass,i})$ referred to as method '*ave*'
(3) $DOD_{ass,i+1} = DOD_{list}(i+1)$ referred to as method '*list*'

The vector DOD_{list} contains a list of predefined values the algorithm iterates over. Since the methods *last* and *ave* not necessarily employ the full range of possible DOD values they can get stuck in a 'local optimum' and are therefore technically defined as heuristic. For the *list* method this risk can be eliminated by choosing the list over which is iterated such that it describes the full range of possible DOD values. The fourth method is to apply the linear approximation of the red curve in Figure 3.2b, referred to as method '*lin*'.

3.3.2 SOC-related degradation

Average SOC is the second factor we discuss. The degradation function that accounts for the loss in capacity attributable to the average SOC-level is described by

a linear fit on data of 15-year capacity versus average SOC (Markel, Smith, and Pesaran, 2009; Hoke et al., 2011). Various 24-hour battery data profiles were fed in the NREL-model and data of relatively lost lifetimes versus average SOC during one hour were obtained. The conditions and assumptions under which the data were obtained are unknown, but they are assumed to sufficiently resemble the framework of this research. It is imported to note that degradation due to SOC-level is usually associated with calendar aging. However, as the authors recognize, the average SOC during a battery cycle, i.e. during operation, also has an impact on cycle life degradation. All used battery profiles had constant low temperature (6 °C) to diminish the temperature effect. The fitted formula for the degradation due to one hour of average SOC equal to SOC_{avg} has the following form.

$$\frac{\Delta L_{SOC}}{L} = \frac{h \cdot SOC_{avg} - l}{CF_{max} \cdot 15 \cdot 8760} \tag{3.7}$$

CF_{max} denotes the maximum capacity fade at EOL (in this research denoted by ζ) and $15 \cdot 8760$ is the amount of hours in 15 years. It is assumed that storing a battery at an SOC-level of SOC_{avg} has similar degradation effects as one hour of battery use during which the average SOC-level is equal to SOC_{avg}. Since this research focuses on one day (or 24 hours) of operation, the degradation function (3.7) is multiplied by 24, resulting in the following SOC-dependent degradation function.

$$\frac{\Delta L_{SOC}}{L} = 24 \cdot \left(\frac{h \cdot SOC_{avg} - l}{\zeta \cdot 15 \cdot 8760} \right) \tag{3.8}$$

3.3.3 Temperature-related degradation

Lastly the degradation related to battery temperature is explained. The internal temperature of a battery varies with the power it is charged or discharged at. Only the degradation during charging is considered, since the battery temperature during discharging is independent of the decisions involved in the problem. Also only the *extra* degradation due to fast-charging is considered, compared to the degradation of charging at lowest possible power. This combined with the knowledge that temperature mainly affects calendar aging the contribution of temperature to the total degradation has the least contribution to total degradation (Hoke et al., 2011).

To correctly calculate the degradation, the lifetime loss attributed to charging should be compensated for the loss that would have been generated by charging in the least harmful way possible, since charging must happen anyhow. Charging in the least harmful way possible is defined as a constant power charge at minimum power P_{min} required to fully charge the battery in the available time t_{max}. The relation between temperature and power during charging can be expressed linearly as follows:

$$T = T_{amb} + R_{th} \cdot P,$$

where T_{amb} is the ambient temperature, R_{th} the thermal resistance of the battery and P is the applied power (Hoke et al., 2011). The relation between lifetime in years and temperature at which a battery is stored can be expressed as follows.

$$L(T) = a \cdot e^{b/T} \tag{3.9}$$

For temperature-related degradation it is complex to isolate the cycle aging. In general is mostly associated with calendar aging, and is probably the least interesting degradation factor for this research. We will discuss the method of determining

degradation by temperature here, and apply it only to temperature changes due to charging to approximately isolate the effect on cycle life. The relative lifetime loss for one charging opportunity is calculated as follows (Hoke et al., 2011).

$$\frac{\Delta L_{Temp}}{L} = \underbrace{\int_{t_{ch}} \frac{1}{8760 \cdot L\big(T_{amb} + R_{th} \cdot P(t)\big)} \mathrm{d}t}_{\Delta L/L \text{ due to charging}} + \underbrace{\frac{t_{max} - t_{ch}}{8760 \cdot L\big(T_{amb}\big)}}_{\substack{\Delta L/L \text{ while plugged} \\ \text{in but not charging}}} - \underbrace{\frac{t_{max}}{8760 \cdot L\big(T_{amb} + R_{th} \cdot P_{min}\big)}}_{\substack{\text{Baseline } \Delta L/L \text{ that would be} \\ \text{realized due to slow charging}}} \tag{3.10}$$

The factor 8760 is the number of hours in a year and is needed to express the lifetime (in years) in the used units for time t (hours). The used time for charging is expressed by t_{ch}. The resulting cost function (3.10) is designed to only account for degradation that could have been avoided if the least harmful procedure of charging had been employed, i.e. charging at the lowest possible power. The first two parts calculate the lifetime loss for charging at high power, during charging and the rest of the time it would take at the minimum power level to recharge, and the lifetime loss in the least harmful way possible, calculated in the last part of (3.10), is subtracted.

The equation is rather complicated and far from linear, but since the charging profile is similar for all charging stations of the same type under current assumptions, the lifetime loss effect can be determined per type of charging station at every stop. Note that the dwell time are assumed to be completely utilized for charging. The corresponding degradation is only dependent on the installed charging stations of each type. Because of the assumption of constant power during charging, the integral in equation (3.10) can be replaced by a simple expression. The lifetime loss per type of station can now be calculated as follows, using the notation described in Section 3.2.

$$\frac{\Delta L_{Temp,t,s}}{L} = \frac{\delta_s}{\theta_{year} \cdot L(T_{amb} + R_{th} \cdot \pi_s^t)} + \frac{\delta_{depot} - \delta_s}{\theta_{year} \cdot L(T_{amb})} - \frac{\delta_{depot}}{\theta_{year} \cdot L(T_{amb} + R_{th} \cdot \pi_{depot})} \tag{3.11}$$

The total degradation related to temperature can now easily be obtained with the information of what types of stations are installed at which stops. This simplification is only possible because all charging stations are assumed to be equal.

$$\frac{\Delta L_{Temp}}{L} = \sum_{t \in T} \sum_{s \in S} \frac{\Delta L_{Temp,t,s}}{L} \cdot x_s^t \tag{3.12}$$

3.4 Model with Weighted Sum Method

The weighted sum method combines both objectives, minimizing costs as well as battery degradation, in one single objective. Minimizing battery degradation is defined in terms of battery degradation costs, for which we can use the functions described in equation (3.2). The idea is to minimize daily costs, by dividing initial investment cost by lifetime in days and calculating degradation costs per day.

3.4.1 The weighted sum method

The traditional approach to solving MOPs of the Pareto class is by scalarization and formulating a single objective optimization problem that is related to the MOP. The simplest method that is based on this idea is the weighted sum method, explained

here in brief (Ehrgott, 2006, Chapter 3). In the weighted sum method, a solution is found for a *weighted sum scalarization* of the MOP. Every involved objective function $f_k(x)$ is appointed a weight λ_k. The resulting objective is of the form

$$\min_{x \in \mathcal{X}} \sum_{k=1}^{p} \lambda_k f_k(x).$$

For the application to this research, only the case of strictly positive weighting vectors is relevant. The assumption of $\sum_{k=1}^{p} \lambda_k = 1$ always holds, since this just normalizes the weights.

Assume we have an MOP with two objective functions $y_1 = f_1(x)$ and $y_2 = f_2(x)$ and feasible region $\mathcal{X}$. The set of feasible objective values is defined as

$$\mathcal{Y} = \{(f_1(x), f_2(x)) | x \in \mathcal{X}\}.$$

The space of which $\mathcal{X}$ is a subset is referred to as the *decision space* and the space of which $\mathcal{Y}$ is a subset is referred to as the *objective space*. In this case the objective space is defined on $\mathbb{R}^2$ and $\mathcal{Y}$ can therefore be imaged in a two-dimensional graph. In Figure 3.3 an illustrative example of the visualization of a set of feasible objective values $\mathcal{Y}$ is depicted.

In this example the weighted sum results in the family of lines $\{y \in \mathbb{R}^2 | \lambda_1 y_1 + \lambda_2 y_2 = c, c \in \mathbb{R}\}$. The new optimization problem is now defined by finding the minimum value for $c = \hat{c}$ such that the intersection of the line with $\mathcal{Y}$ is nonempty. The set of points on that intersection, $\hat{y}$, are the optimal points of $\mathcal{Y}$ with respect to λ. To find $\hat{c}$ graphically, we can start with a large value for c and move the line in parallel towards the origin as much as possible while keeping a nonempty intersection with $\mathcal{Y}$. In the example we see that there exist two points that satisfy this requirement, these points are also referred to as *nondominated* solutions. Adjusting the weights will lead to relatively more emphasis on the 'heaviest' of the objectives and can be applied to adjust the relative importance of the objectives to each other.

3.4.2 The MILP model

Employing the weighted sum method and applying the notation described in Section 3.2 results in the following model. λ_{inv} and λ_{deg} denote the weight for the investment and battery life objectives, resp. The weights are assumed to be normalized and positive: $\lambda_{inv} + \lambda_{deg} = 1, \ \lambda_{inv}, \lambda_{deg} > 0$.

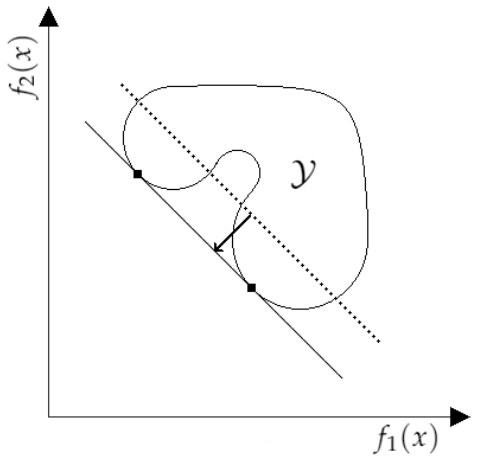

FIGURE 3.3: *Visualization of the weighted sum method*

$$\min \quad \lambda_{inv}\left(\beta \sum_{i\in I} \frac{\Gamma_{batt,i}\cdot b_i}{\eta_{batt,i}} + \sum_{t\in T}\left[\frac{\sum_{s\in S} x_s^t\cdot \Gamma_s^t + \sum_{d\in D} x_d^t\cdot \alpha_d^t}{\eta^t}\right]\right) + \lambda_{deg}\cdot\beta\cdot g_{deg}^{\lambda}(DOD, SOC_{avg}, b) \quad (3.13)$$

$$\begin{aligned}
\text{s.t} \quad z_s &= w_{s-1} - \mu_{s-1} && \forall s\in S\backslash\{1\}, && (3.14)\\
z_s &\geq \textstyle\sum_{i\in I} b_i\cdot\kappa_i\cdot\zeta && \forall s\in S, && (3.15)\\
y_s &\leq \textstyle\sum_{t\in T} x_s^t\cdot\phi_s^t && \forall s\in S, && (3.16)\\
y_s &\leq \textstyle\sum_{t\in T} x_s^t\cdot\delta_s\cdot\pi_s^t && \forall s\in S, && (3.17)\\
w_1 &= \textstyle\sum_{i\in I} b_i\cdot\kappa_i\cdot\omega && , && (3.18)\\
w_s &= z_s + y_s && \forall s\in S, && (3.19)\\
w_s &\leq \textstyle\sum_{i\in I} b_i\cdot\kappa_i\cdot\omega && \forall s\in S, && (3.20)\\
w_s &\geq \textstyle\sum_{i\in I} b_i\cdot\kappa_i\cdot\zeta + \nu_s && \forall s\in S, && (3.21)\\
w_A &= w_1 && , && (3.22)\\
v &\leq z_s && \forall s\in S, && (3.23)\\
\textstyle\sum_{i\in I} b_i &= 1 && , && (3.24)\\
\textstyle\sum_{t\in T} x_s^t &\leq 1 && \forall s\in S, && (3.25)\\
x_s^{TFS} &= 1 && \forall s\in S^{TFS}, && (3.26)\\
x_s^{TFS} &= 0 && \forall s\in S\backslash S^{TFS}, && (3.27)\\
x_d^t &\leq \tfrac{1}{2}\textstyle\sum_{s\in S_d} x_s^t && \forall t\in T,\ \forall d\in D, && (3.28)\\
(\mathcal{P}_{A.1}) \quad h_{dwell,1} &= \tfrac{1}{2}\left(\textstyle\sum_{i\in I} b_i\cdot\kappa_i + w_A - \nu_A\right)\cdot\delta_{depot} && , && (3.29)\\
h_{dwell,s} &= \tfrac{1}{2}\rho(z_s + w_s)\cdot\delta_s && \forall s\in S\backslash\{1\}, && (3.30)\\
h_{travel,s} &= \tfrac{1}{2}\rho(w_s + z_{s+1})\cdot\tau_s && \forall s\in S\backslash\{A\}, && (3.31)\\
h_{travel,A} &= \left(\textstyle\sum_{i\in I} b_i\cdot\kappa_i + w_A - \nu_A\right)\cdot\tau_{depot} && , && (3.32)\\
DOD_i &\geq b_i - \frac{v}{\kappa_i} && \forall i\in I, && (3.33)\\
b_i - SOC_{avg,i} &\leq \frac{\sum_{j\in I} b_j\cdot\kappa_j}{\kappa_i} - \frac{\sum_{s\in S}\left[h_{dwell,s} + h_{travel,s}\right]}{\kappa_i\cdot\theta_{day}} && \forall i\in I, && (3.34)\\
x_s^t &\in \{0,1\} && \forall t\in T,\ \forall s\in S, && (3.35)\\
x_d^t &\in \{0,1\} && \forall t\in T,\ \forall d\in D, && (3.36)\\
b_i &\in \{0,1\} && \forall i\in I, && (3.37)\\
w_s,\ y_s,\ z_s &\geq 0 && \forall s\in S, && (3.38)\\
v &\geq 0 && , && (3.39)\\
h_{j,s} &\geq 0 && \forall j\in\{dwell, travel\},\ \forall s\in S, && (3.40)\\
DOD_i &\geq 0 && \forall i\in I, && (3.41)\\
SOC_{avg,i} &\geq 0 && \forall i\in I. && (3.42)
\end{aligned}$$

This formulation is further referred to as model $A.1$. The objective function (3.13) consists of two parts, the capital investment for on-board batteries and charging station installment and a battery lifetime part expressed by degradation costs. The investment costs are divided by respective lifetime in days (under ideal conditions) because the degradation is calculated as relative lifetime loss per operation days as well. In that way both objectives are expressed in a comparable manner. The costs

of buses are left out of scope, since they are independent of decisions made by the model. The degradation costs can be viewed as a penalty incurred for extra lifetime loss for less-than-ideal conditions. The degradation costs are expressed as follows.

$$g^{\lambda}_{deg}(DOD, SOC_{avg}, b) = g^{\lambda,SOC}_{deg}(SOC_{avg}, b) + g^{\lambda,DOD}_{deg}(DOD, b) \tag{3.43}$$

$$g^{\lambda,SOC}_{deg}(SOC_{avg}, b) = 24 \cdot \gamma_{batt} \cdot \left(\frac{\sum_{i \in I} \left[\kappa_i \cdot (h \cdot SOC_{avg,i} - l \cdot b_i) \right]}{\zeta \cdot 15 \cdot 8760} \right) \tag{3.44}$$

$$g^{\lambda,DOD}_{deg}(DOD, b) = \gamma_{batt} \cdot \sum_{i \in I} \left[\kappa_i \cdot (m \cdot DOD_i + n \cdot b_i) \right] \tag{3.45}$$

Unfortunately, because the concept of degradation costs is applied, it is impossible to incorporate temperature related degradation. The battery costs are directly related to the battery size, which is a variable in the model. The outcome of multiplying the battery costs with temperature related degradation, which is a function of variable x^t_s, see equation (3.12), would be a non-linear function and is thus not suited for an MILP. However, temperature degradation is of the least interest for this research, as it is associated to calendar ageing, so the impact on the solutions will be minor.

For SOC and DOD related degradation this problem does not arise, since DOD and SOC are represented in the model for every possible battery size separately. This was necessary because both are expressed as fraction of the battery capacity. Only the variables corresponding to the battery size that is chosen in the model are set to their true value, for other configurations the SOC and DOD variables are set to 0.

Constraints (3.14) describe the battery level upon arriving at a stop and constraints (3.15) ensure it is never inferior to the imposed lower bound. Constraints (3.16) and (3.17) limit the energy that can be charged when a charging facility is placed by its power and maximum available energy to charge at a time. Constraint (3.18) initializes the energy level and (3.19)-(3.21) describe the energy in the battery upon leaving a stop and bound it by the imposed upper bound and required energy to reach the depot. Constraint (3.22) ensures that the energy level at the end of a round trip equals the energy level at the start to satisfy the assumption that a full operation day can be described by one bus cycle.

Constraints (3.23) represent the minimum battery level that is reached on a day, which is required to determine the depth of discharge. Constraint (3.24) enforce

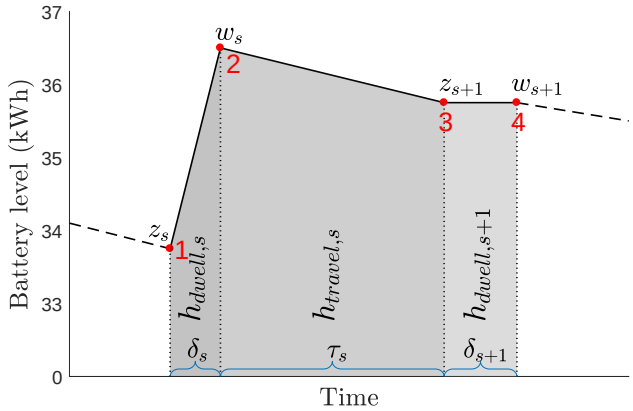

FIGURE 3.4: *An illustration of the auxiliary* **h** *variables for determining average SOC. The points indicate events 1. arrival at bus stop* **s** *with charging facility, 2. departure from bus stop* **s**, *3. arrival at bus stop* $\mathbf{s} + \mathbf{1}$ *without charging facility, 4. departure from bus stop* $\mathbf{s} + \mathbf{1}$.

a single option of battery size and constraints (3.25)-(3.27) ascertain that at most one charging facility is placed at every stop, enforcing TFS at all terminal stops. Constraints (3.28) set the value of x_d^t to 1 only if a station of type t is installed in both directions of stop d.

Constraints (3.29)-(3.32) calculate the auxiliary variables required to determine the average SOC. These variables represent the area under the energy level graph over time, as is depicted in Figure 3.4. A more elaborate description and derivation of these variables can be found in Appendix A.

Constraints (3.33) calculate the depth of discharge for every battery size. Only for the battery size that is chosen, and $b_i = 1$, will the DOD_i variable be equal to the depth of discharge imposed by the solution. For all other battery sizes the right-hand side of the equation will be less than 0 and corresponding DOD_i will be set to 0 since degradation, and thus the objective function, is increasing in DOD.

Constraints (3.34) calculate the average state of charge over a full day of operation (24 hours). Again the value is calculated for every battery size separately and again only for the battery size that is chosen will the variable be equal to the average SOC corresponding to the solution. This expression appears to be unnecessarily complicated, but is required to be of this form because of different possible battery sizes. It is further explained in Appendix A. Constraints (3.35)-(3.42) represent the domain constraints.

3.5 Model with ε-constraint Method

Another approach, using the ε-constraint method, is presented in this Section. Similar to the weighted sum method, the problem is reduced to a single objective optimization problem. However, it does not require to aggregate objectives in one expression and thus it is not necessary to translate battery degradation into costs. With the ε-constraint method one of the involved objectives is optimized and the others are introduced in the problem as a constraint. The idea is to minimize the investment costs, accounted to daily costs, and impose a restriction on the loss in battery life.

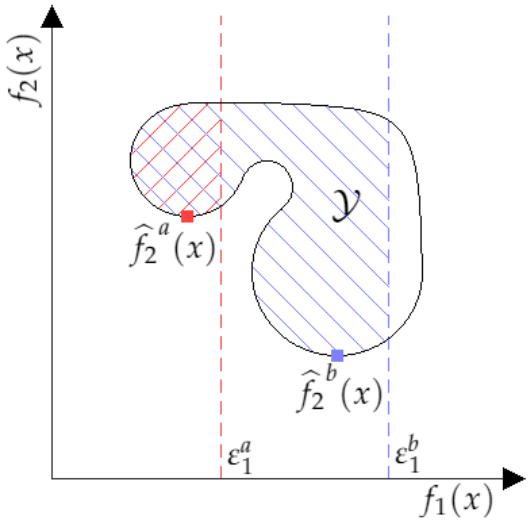

FIGURE 3.5: *Visualization of the ε-constraint method, with two examples of ε-constraints for $f_1(x)$. The resulting sets of feasible objective values are represented by the areas marked in the same color and the corresponding solutions are highlighted.*

3.5.1 The ε-constraint method

The ε-constraint method is a renowned technique in the field of multicriteria optimization problems. Instead of aggregating the involved objectives, only one of them is optimized and the others are moved to the constraints. The MOP defined in expression (3.1) is substituted by the ε-constraint problem (3.46).

$$\begin{aligned} &\min_{x \in \mathcal{X}} f_j(x) \\ &\text{s.t. } f_k(x) \leq \varepsilon_k \qquad k = 1, \ldots, p \quad k \neq j \end{aligned} \tag{3.46}$$

For illustration, again consider an MOP with two objectives, $f_1(x)$ and $f_2(x)$ and take $j = 2$, so an upper bound constraint is put on $f_1(x)$. A visualization of the method can be seen in Figure 3.5. The feasible set of objective values $\mathcal{Y}$ is depicted with two various values for ε_1. As can be seen in the figure, each choice for ε_1 reduces the area of $\mathcal{Y}$, and thus affects the set of values that $f_2(x)$ can assume. The resulting optimal values $\widehat{f}_2(x)$ are marked. Adjusting the ε-values for the objectives in the constraints will thus result in a 'tighter' or a 'looser' set of feasible objective values $\mathcal{Y}$ and is a tool for controlling the problem on hand. For a more elaborate explanation on the ε-constraint method and further results and theory, the reader is referred to further literature on the ε-constraint method (e.g. Haimes, Lasdon, and Wismer, 1971; Chankong and Haimes, 1983; Ehrgott, 2006, Chapter 4.1).

3.5.2 The MILP model

As was mentioned above, the investment costs are handled as primary objective, leaving the battery life objective represented in the constraints. The restriction on the battery life degradation is denoted with ε_{deg}. Apart from the adjustment of the objective function and the addition of the ε-constraint the model is equal to model $A.1$. The objective function and ε-constraint are as follows

$$\min \quad \beta \sum_{i \in I} \frac{\Gamma_{batt,i} \cdot b_i}{\eta_{batt,i}} + \sum_{t \in T} \left[\frac{\sum_{s \in S} x_s^t \cdot \Gamma_s^t + \sum_{d \in D} x_d^t \cdot \alpha_d^t}{\eta^t} \right] \tag{3.47}$$

$$\text{s.t} \qquad \varepsilon_{deg} \quad \geq \quad \beta \cdot g_{deg}^{\varepsilon}\left(DOD, SOC_{avg}, x\right) \tag{3.48}$$

This formulation is further referred to as model $B.1$. Including temperature degradation is possible with this formulation, since the battery size is not involved. The involved degradation functions are the expressed as follows.

$$g_{deg}^{\varepsilon}\left(DOD, SOC_{avg}, x\right) = g_{deg}^{\varepsilon,SOC}\left(SOC_{avg}\right) + g_{deg}^{\varepsilon,DOD}\left(DOD\right) + g_{deg}^{\varepsilon,Temp}\left(x\right) \tag{3.49}$$

$$g_{deg}^{\varepsilon,SOC}(SOC_{avg}) = 24 \cdot \left(\frac{h \cdot \sum_{i \in I} SOC_{avg,i} - l}{\zeta \cdot 15 \cdot 8760} \right) \tag{3.50}$$

$$g_{deg}^{\varepsilon,DOD}(DOD) = m \cdot \sum_{i \in I} DOD_i + n \tag{3.51}$$

$$g_{deg}^{\varepsilon,Temp}(x) = \sum_{s \in S} \sum_{t \in T} \frac{\Delta L_{Temp,t,s}}{L} \cdot x_s^t \tag{3.52}$$

3.6 Extensions

To improve the solutions and better approximate real operating conditions a few extensions to the model are proposed in this Section.

3.6.1 Possibility for energy depletion in every cycle

Although it was assumed that an operation day can be fully described by a single bus cycle, there might be opportunities for a better solution if the SOC was able to slowly decrease with every bus cycle, i.e. relaxing the assumption of equal battery level at the start and end of each bus cycle. In models $A.1$ and $B.1$ the batteries are forced to be fully recharged at the end of every bus cycle. It is valuable to research the added value of allowing more freedom for the energy level development over the day.

In order to model this freedom an extra variable is introduced e_{cycle}, which denotes the *used energy per bus cycle*, and can be calculated as the difference between the starting and ending energy level of one bus cycle.

$$e_{cycle} = w_1 - w_A \tag{3.53}$$

The constraints involved with lower bound on the energy level are reduced with $(\rho - 1) \cdot energy_{cycle}$ to assure that these restrictions are also met during the last bus cycle. An example of such a constraint:

$$z_s \geq \sum_{i \in I} b_i \cdot \kappa_i \cdot \zeta + (\rho - 1) \cdot e_{cycle} \tag{3.54}$$

The calculation of the average SOC needs to be adjusted to account for the gradual decrease in battery level over the day. The total time to complete one bus cycle is also required and will be denoted by θ_{cycle}. After incorporating the variable e_{cycle}, the SOC constraint is expressed as follows.

$$b_i - SOC_{avg,i} \leq \frac{\sum_{j \in I} b_j \cdot \kappa_j}{\kappa_i} - \frac{\sum_{s \in S} \left[h_{dwell,s} + h_{travel,s}\right] - \frac{1}{2}(\rho^2 - \rho)\theta_{cycle} e_{cycle}}{\kappa_i \cdot \theta_{day}} \tag{3.55}$$

An explanation and derivation of this expression can be found in Appendix A. The complete MILPs can be found in Appendix B. These models are further referred to as $A.2$ and $B.2$, or in general as $X.2$.

3.6.2 Optimizing charging policy

The first proposed extension adds the possibility of a decrease in battery level after every bus cycle. However, it has the limitation of imposing the same charging decisions for every bus cycle, i.e., charging the same amount of energy every time the same charging station is visited. With regard of battery degradation optimization it might be beneficial to let these decisions differ for every charging opportunity, i.e. relaxing the assumption that the daily operation can be described by one bus cycle.

The models $A.1$ and $B.1$ are the basis for this extension. In order to allow for variations in charging decision it is necessary to create a copy for every stop for every bus cycle. This significantly increases the number of nodes in the graph and thus the size of the problem. The number of stops during one bus cycle is denoted by N and the total number of nodes in the model is again denoted by A (note that

$A = \rho \cdot N + 1$). To ensure that the installment of stations along the route is the same for all copies of the stops, the following constraint is added.

$$x_s^t = x_{s-N}^t, \qquad \forall t \in T, \forall s \in S, s > N \tag{3.56}$$

Besides this addition and some minor adjustments, the formulations of the original models support this extension sufficiently. The models with this extension are referred to as $A.3$ and $B.3$, or in general as $X.3$. The complete MILPs can be found in Appendix B.

Chapter 4

Data

In order to test the developed models input parameters for degradation functions and technical features are required. Due to confidentiality of exact technological features, for competition and pending patent reasons, parameters from a manufacturer source were unavailable. Therefore the parameters were obtained from literature. The applicability to the problem and the feasibility of the combination of the used parameters might not be completely technically valid. Nevertheless, the main goal of this thesis is the development of a universal model for the design of a charging network and the chosen values of the parameters do not need to exactly describe one type of scenario. It is assumed that these parameters are sufficient for a universal model. The used parameters and their source are described in Section 4.1. Data for a bus line is synthesized based on an operated bus line in Rotterdam, using distances between stops to calculate energy consumptions and travel times. This is described in Section 4.2.

4.1 Parameters

First the source of the parameters per degradation function is described and the conditions under which they hold are stated if they were reported. An overview of the parameters can be found in Table 4.1.

DOD degradation For DOD degradation the required parameters are d and f for the cycle lifetime equation (3.3). These values were obtained from Hoke et al. (2011), that fitted the formula on data from Rosenkranz (2003) for lithium-ion battery technology. The data was unobtainable, so it remains unknown what the conditions of the battery were. However, we do know that the assumed EOL capacity is 80%, similar to the assumption in this research. Other conditions are assumed to be sufficiently comparable, the provided parameter values are $d = 145.71$ and $f = -1/0.6844$. The parameters for the degradation function, m and n, are iteratively obtained during the optimization process described in Algorithm 1.

SOC degradation The required parameters for SOC degradation function (3.8) are h and l and were obtained from Hoke et al. (2011). The coefficients were tuned by fitting a linear function on data of average SOC vs. relative lifetime loss. This means that the denominator of equation (3.8) already includes the reported coefficients. Only data points for which average SOC exceeded 0.6 were used for the fit to eliminate effects of high DOD that generally coincide with low SOC averages. They assumed a maximum capacity fade of $CF_{max} = 0.20$ and reported parameters $h^* = 1.59 \cdot 10^{-5}$ and $l^* = 6.41 \cdot 10^{-6}$, which after adjustment for the denominator take the values $h = 0.4179$ and $l = 0.1685$.

Temperature degradation The parameters a and b for the temperature lifetime equation (3.9) are determined by fitting the formula to data obtained from the NREL battery degradation model (Hoke et al., 2011). The authors note that for different DOD-profiles fed into the NREL model, different parameters for $L(T)$ were found, but none of them are reported. The exact same degradation function is used in Barco et al. (2017), and they report parameters $a = 3.73 \cdot 10^{-4}$ and $b = 636$, but the circumstances and assumptions are not mentioned. Nevertheless, the conditions are assumed to match the framework of this problem and these parameter values are used to calculate $L(T)$. Values $T_{amb} = 25\,^{\circ}\text{C}$ and $R_{th} = 4 \cdot 10^{-5}$ were obtained from Hoke et al. (2011).

Other parameters The rest of the parameters that can be found in Table 4.1 were either based on the assumptions that frame the problem (e.g. ζ and ω values), or averaged over publicly available information about running projects for fast-charging electric buses (Pihlatie and Paakkinen, 2017). Information regarding price and lifetime of batteries and charging stations is dependent on the supplier chosen for the batteries and charging equipment. For this research the used prices were obtained from a paper that analyzed costs for various suppliers and averaged over them (Lajunen, 2014). The time (2014) and place (Western-Europe) that frame this research are assumed to be sufficiently analogous to the setting of this research and adjustments for inflation or location are unnecessary.

4.1.1 Values for λ and ε

The two different methods for solving MOPs require the parameters λ_{inv} and λ_{deg} for the weighted sum method, and ε for the ε-constraint method. The λ-values define the relative dominance of the objectives and the tendency of the solution to prioritize one over the other. At first both objectives will be set equally important ($\lambda_{inv} =$

Parameter	*Value*	*Source*
a	$3.73 \cdot 10^{-4}$	Barco et al. (2017)
b	636	Barco et al. (2017)
d	145.71	Hoke et al. (2011)
f	$-1/0.6844$	Hoke et al. (2011)
h	0.4179	Hoke et al. (2011)
l	0.1685	Hoke et al. (2011)
T_{amb}	25 °C	Hoke et al. (2011)
R_{th}	$4 \cdot 10^{-5}$ °C/W	Hoke et al. (2011)
$\pi_s^{FFS}/\pi_s^{SFS}/\pi_s^{TFS}/\pi_{depot}$	600/200/100/50 kW $\forall s \in S$	Pihlatie and Paakkinen (2017)
$\phi_s^{FFS}/\phi_s^{SFS}/\phi_s^{TFS}$	10.0/2.0/5.0 kWh $\forall s \in S$	Pihlatie and Paakkinen (2017)
ζ	0.20	Assumptions (Section 2.2.1)
ω	0.90	Assumptions (Section 2.2.1)
κ_i	$i \cdot 5$ kWh, $i = 1, \ldots, 16$	Assumptions (Section 2.2.1)
γ_{batt}	1000 €/kWh	Lajunen (2014)
$\Gamma_s^{FFS}/\alpha_d^{FFS}$	€200,000/-€100,000 $\forall s \in S$	Lajunen (2014)
$\Gamma_s^{SFS}/\alpha_d^{SFS}$	€150,000/-€75,000 $\forall s \in S$	Lajunen (2014)
$\Gamma_s^{TFS}/\alpha_d^{TFS}$	€120,000/-€120,000 $\forall s \in S$	Lajunen (2014)
$\eta^{FFS}/\eta^{SFS}/\eta^{TFS}/\eta_{batt}$	4,380/4,380/4,380/3,650 days	Lajunen (2014)

TABLE 4.1: *Overview of parameter values*

$\lambda_{deg} = 0.5$). The impact of the parameter values on the solution is evaluated in Chapter 5. The ε-value limits the battery degradation per day to a preset maximum and the solutions obtained with various values are compared.

4.2 Synthesized Bus Line

The bus line data used to evaluate the performance of the model are synthesized based on bus line 33 in Rotterdam which travels between the airport and the main railway station, see Figures 4.1 and 4.2. This bus line is operated daily between 06:00 a.m. and midnight, 6 times per hour between 07:00 a.m. and 06:30 p.m. and 4 times per hour outside said interval, summing to 96 round trips per day. One round trip (back and forth) takes 51 minutes, so technically a fleet of 6 buses would suffice to operate this bus line and the fleet size is therefore set at $\beta = 6$. In reality it is likely a public transport company would have a slightly larger fleet in order to react to possible defects and delays, but this would be of concern in a scenario of multi-line network optimization. The round trips are assumed to be equally divided among the fleet, resulting in a value for $\rho = 16$.

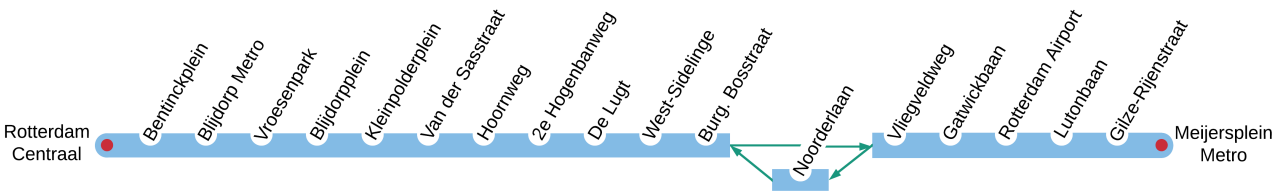

FIGURE 4.1: *Graphical depiction of all the stops on bus line 33*

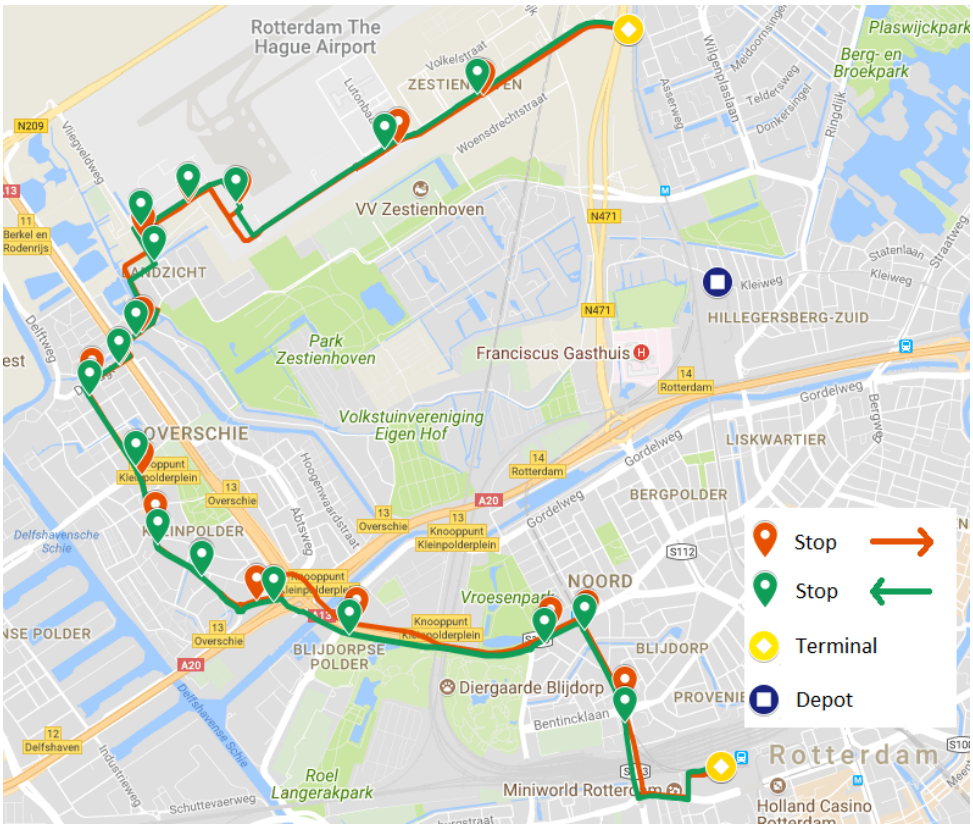

FIGURE 4.2: *Bus line 33 depicted on the map*

4.2.1 Energy consumption and travel time

The only information available to estimate energy consumption and travel time were the distances between stops, obtained from Google Maps. To calculate power consumption between consecutive stops i and j at a given time t, $P_{i,j}(t)$, it was separated in three different terms involved in the overall consumption (Barco et al., 2017).

$$P_{i,j}(t) = \frac{P_{aerodynamic}(t) + P_{rolling}(t) + P_{accelerate}(t)}{\hat{\eta}} \tag{4.1}$$

The terms in equation (4.1) respectively denote the power depleted by aerodynamic drag, by rolling resistance between tires and asphalt and to overcome the vehicle inertia for acceleration/deceleration. The terms are summed and divided by the powertrain efficiency of the bus ($\hat{\eta}$) to find the power consumption. A fourth possible term corresponds to power that is consumed or gained as a result of the road grade (in other words, by driving up or down a hill). This term is omitted here because the road grades are unknown. Generally the road grades are negligible in the road network of Rotterdam, so this will not have great impact on the power consumption calculation. If we substitute corresponding formula's for the various power consumptions in equation (4.1) we get the following equation.

$$P_{i,j}(t) = \frac{\frac{1}{2}\rho_{air} A_f c_d [s_{ij}(t)]^3 + m_v g c_r s_{ij}(t) + m_v \left| \frac{\mathrm{d}s_{ij}(t)}{\mathrm{d}t} \right| s_{ij}(t)}{\hat{\eta}} \tag{4.2}$$

The vehicle characteristics required for this calculation are described in Table 4.2. The speed at time t, denoted by $s_{ij}(t)$ can be derived from the speed profile associated with the road sections between stops i and j. However, speed profiles between consecutive stops are unknown. The associated speed profiles of the route sections are simplistically derived by splitting them in three phases: acceleration, constant speed and deceleration; referred to as phase I, phase II and phase III respectively. In phase I the bus accelerates linearly up to an average velocity, during phase II it retains that velocity and in phase III, starting from the moment it needs to brake in order to stop in time at the next stop, it decelerates linearly to standstill.

The speed limit along the route is 50km/h, but it is unlikely that the average speed during phase II is equal to the speed limit. Using the openly available speed profile for roads in the Netherlands from Spotzi B.V. and TomTom, we see the average speeds of the sections along the route of bus line 33 lie between 30 and 50km/h (Spotzi B.V. and TomTom, 2013). The assumed average speed during the constant speed phase is therefore set at 40km/h, or $v = 11.11\mathrm{m/s}$. The rate of acceleration is assumed to be $r_a = 0.7\mathrm{m/s^2}$ and the rate of deceleration/braking is assumed to be $r_d = 1.0\mathrm{m/s^2}$. Assuming $t = 0$ at the beginning of every phase, the corresponding speed profiles can be expressed as follows.

$$s_{ij}^{I}(t) = r_a \cdot t, \qquad s_{ij}^{II}(t) = v, \qquad s_{ij}^{III}(t) = v - r_d \cdot t$$

The travel times τ_i between consecutive stops can now easily be derived. The time spent in each phase is denoted by τ_i^I, τ_i^{II} and τ_i^{III}. The energy consumptions between consecutive stops i and j can be found by integrating equation (4.2) over time t (see Appendix C).

$$\mu_i = \int_0^{\tau_i^I} P_{i,j}(t)\mathrm{d}t + \int_0^{\tau_i^{II}} P_{i,j}(t)\mathrm{d}t + \int_0^{\tau_i^{III}} P_{i,j}(t)\mathrm{d}t \tag{4.3}$$

Parameter	*Description*	*Value*	*Source*
ρ_{air}	Air density	1.184kg/m^3	physical constant (for T =25 °C)
A_f	Frontal area	7.74m^2	X. Hu et al. (2013)
c_d	Aerodynamic drag coeff.	0.7	X. Hu et al. (2013)
m_v	Vehicle mass	14.5 ton	X. Hu et al. (2013)
g	Gravitational acceleration	9.81m/s^2	physical constant
c_r	Rolling resistance coeff.	0.007	X. Hu et al. (2013)
$\hat{\eta}$	Powertrain efficiency	74%	Pihlatie, Kukkonen, et al. (2014)

TABLE 4.2: *Vehicle characteristics used to determine energy consumption*

4.2.2 Dwell times

According to literature on dwell time modeling, dwell times can be described by a 'dead time', needed to open and close the door, plus a fixed time for every passenger (dis)embarking. Tirachini (2013) provide an overview of literature describing such dwell time models, reporting dead times ranging from 2-16s and additional times per passenger ranging from 0.5-6.9s. The values for the dead time and time per passenger depend on vehicle-, stop- and passengercharacteristics, e.g. door width, number of doors, type of fare collection, relative platform height, passenger age, sequential or simultaneous embarking and disembarking. (Dueker et al., 2004; Fernández et al., 2010, i.a)

Unfortunately we do not have access to such data, so another approach is chosen. The dwell times were obtained from a normal distribution. For terminal stops a different normal distribution was used, since generally dwell times tend to be longer at terminal stations. Using $N(\mu, \sigma)$ as notation for a normal distribution and its average and standard deviation, the used distributions were $N(15, 5)$ for dwell times along the route and $N(210, 70)$ for dwell times at terminal stations. The dwell time at the terminal at the end of a bus cycle was set to be such that the total duration of one bus cycle is exactly one hour. See Figure 4.3 for a visualization of the dwell times.

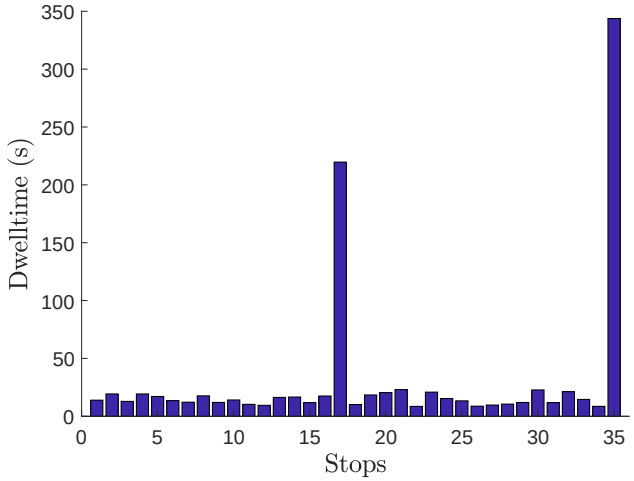

FIGURE 4.3: *Visualization of the dwell times, the two peaks represent the dwell times at terminal stations.*

Chapter 5

Results

In this Chapter the performance of the models will be evaluated. First the performance of the various DOD degradation approximation methods is evaluated in Section 5.1. The two methods for solving MOPs applied to this problem are evaluated in Section 5.2. In Section 5.3 the obtained solutions are compared and the added value of the model, compared to models without integrated battery degradation, is quantified. The contribution of the different degradation factors to battery lifetime is described in Section 5.4 and some sensitivity analysis on their relative influence is performed. All results were obtained with IBM CPLEX-solver software on a Windows computer with a 3.5 GHz processor with 2 CPU and 6 GPU cores, model type 'AMD PRO A6-9500 R5', and 16 GB of installed RAM memory.

5.1 DOD Degradation Approximation Methods

Since four different methods were used for the DOD degradation, i.e. '*ave*', '*last*', '*list*' and '*lin*', they are evaluated and compared here. The first three methods correspond to the iterative solution algorithm. An overview of their performance for solving model $A.1$ for various values of λ_{inv} can be found in Figure 5.1. In the running time graph the method '*lin*' is depicted as well to serve as benchmark.

From the Figures 5.1a-5.1c it is clear that in terms of solving speed the '*last*' method outperforms the other two. This is in line with expectations because choosing the last solution DOD in the next iteration is bound to converge quicker to a solution. However, this also highlights the pitfall of this method. It might be sensitive to the risk of jumping over the DOD-value of the optimal solution as it is considerably greedy. This concern is confirmed by the fact that for one instance of λ_{inv}, the '*last*' method failed to find the optimal solution. This is visualized in Figure 5.1d, where the difference in objective values for '*last*' and '*list*' methods is depicted (between objective values of '*list*' and '*ave*' method the difference was 0 for all λ_{inv} values). Because the domain of DOD-values is closed and bounded (it always falls between 0 and 1) this characteristic might not apply to the method '*list*' if the values in the list sufficiently represent the range of values for DOD, i.e. with small enough difference between consecutive values. Therefore method '*list*' is used for obtaining further results with the iterative solution algorithm.

The fourth method employs a linear approximation of the degradation curve, depicted in Figure 5.2. This is significantly faster than the iterative method (see Figure 5.1c), but has the disadvantage of lower accuracy of the true degradation. The various formulas describing battery degradation due to DOD-cycles are already an approximation of the degradation effect, and further simplification is questionable. Although it is still an approximation, the DOD degradation calculated according to the formulas derived from (3.5) are called 'true degradation' and the linear approximation will be referred to as 'approximated degradation'.

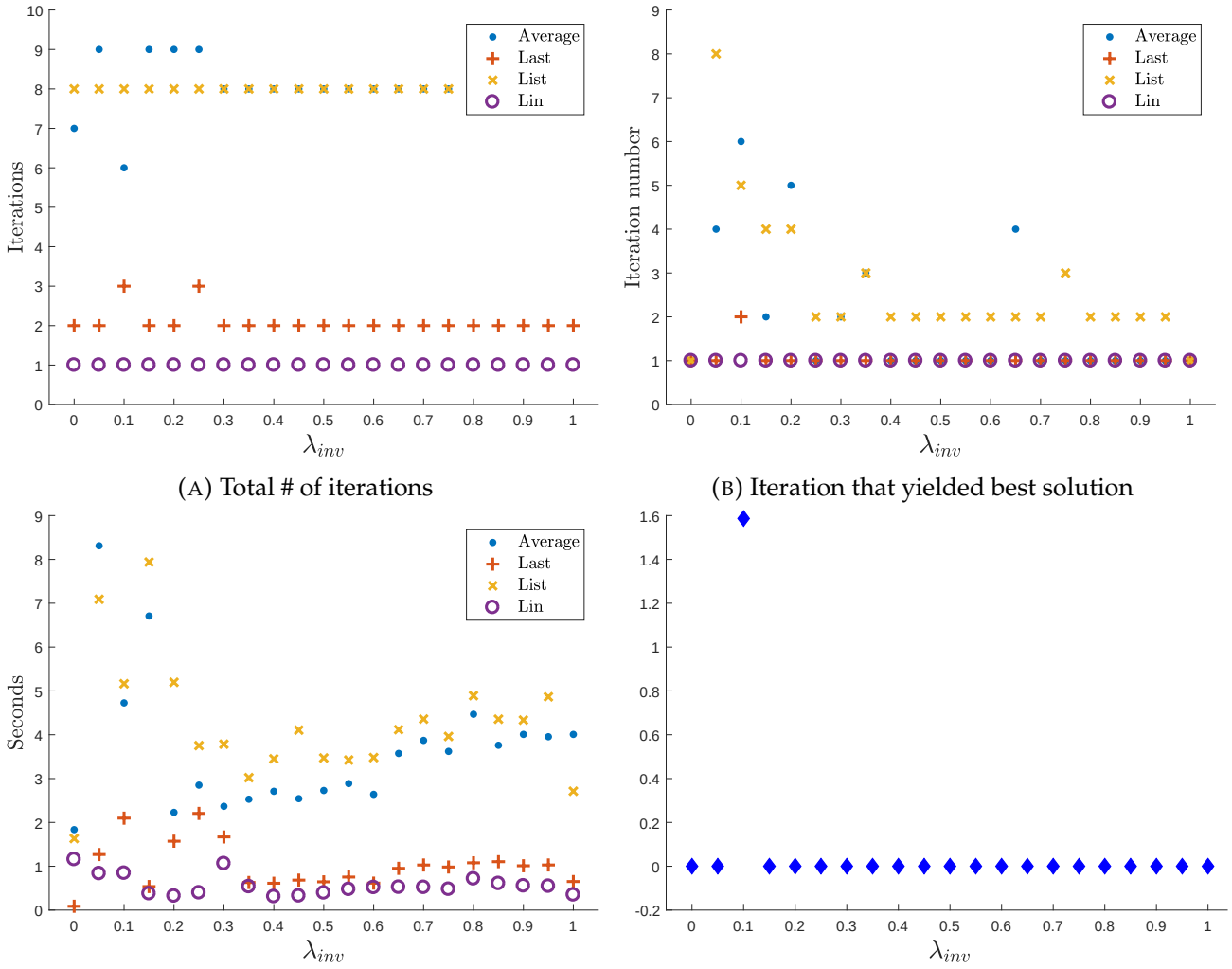

(A) Total # of iterations

(B) Iteration that yielded best solution

(C) Running time in seconds

(D) Difference in obj. values (*last-list*)

FIGURE 5.1: *Comparison of solving performance for the A.1 model, utilizing the different iteration methods used to approximate DOD degradation*

Table 5.1 displays the differences between solutions with true and approximated degradation for $A.1$ models. In the instance for $\lambda_{inv} = 0.25$ both methods found a different solution, and if the DOD-degradation of the '*lin*' method is adjusted to its true value in order to compare both objectives, there is a slight difference of 0.135% in objective value in favor of the '*list*' method. For all other instances both methods found the exact same solutions and the relative differences in DOD-degradation seem to be minor.

However, it is difficult to determine the exact effect on lifetime estimation because lifetime is inversely related to degradation. Smaller degradation values imply longer lifetimes, and therefore a small deviation when the degradation value is low can have more extreme effects for the lifetime estimation in comparison to higher degradation values. This is especially relevant for the ε-constraint method where the degradation is bounded by a parameter in the model and choosing smaller values for ε might induce larger inaccuracies of the model when the linear approximation of DOD degradation is applied.

The overall solving speed of these models is remarkably fast (under 10 seconds for all instances of $A.1$, regardless of the method) and applying a 'quick fix' such as

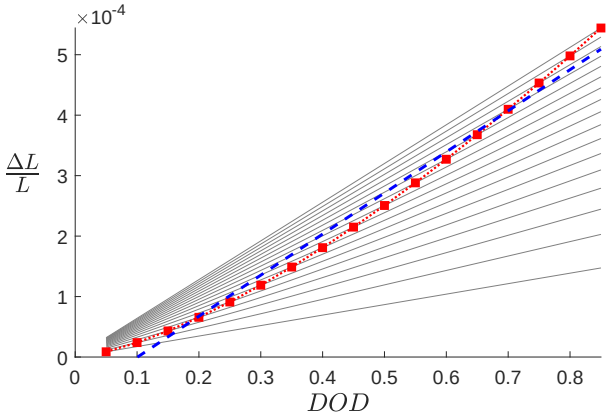

FIGURE 5.2: *Linear approximation of DOD degradation, corresponding to* 'lin' *method*

λ_{inv}	**degr. diff.**
0.05	-3.695%
0.10	3.037%
0.15	-1.476%
0.20	-1.476%
0.25	9.812%
0.30	0.678%
0.35	0.678%
0.40	0.678%
0.45	0.678%
0.50	0.678%
0.55	0.678%
0.60	0.678%
0.65	0.678%
0.70	0.678%
0.75	0.678%
0.80	0.678%
0.85	0.678%
0.90	0.678%
0.95	0.678%
1.00	-0.413%

TABLE 5.1: *Differences in DOD degradation and objective value of solutions found using* 'list' *and* 'lin' *methods*

the linear approximation might seem irrelevant. This fast solving speed, however, is a result of the relative simplicity of the model in its current form. The only true decisions the model is required to take are the size of the on-board batteries and the placement of stations. All other variables in the model take on values as a consequence of these decisions. Furthermore, the fleet was assumed to be homogeneous, and the network only exists of one bus line. Since battery size is determined by binary variables and only two types of stations for all non-terminal stops were introduced, the number of possible solutions is relatively small.

For application to a real bus network design problem, the total number of possible solutions is bound to be significantly larger. It is likely it will involve multiple bus lines, operated by a heterogeneous fleet, and a greater range of possible configurations for charging stations. This will significantly increase the time required to solve the problem. The linear approximation method might be useful to find a solution in that case. For further results the *'list'* method was used to obtain solutions, unless stated otherwise.

5.2 MOP Methods

The results of the two different methods for solving MOPs are discussed here and their performance is evaluated and compared.

5.2.1 Results with weighted sum method

First the results of the weighted sum method, i.e. the A.x models, are discussed. In Figure 5.3 the solutions for various values of λ_{inv} are schematically depicted. The graphs provide an overview of the solutions' costs for the batteries and stations and the expected lifetime of the batteries based on the degradation corresponding to the solutions. Note that the lifetime is expressed in operation days since we are

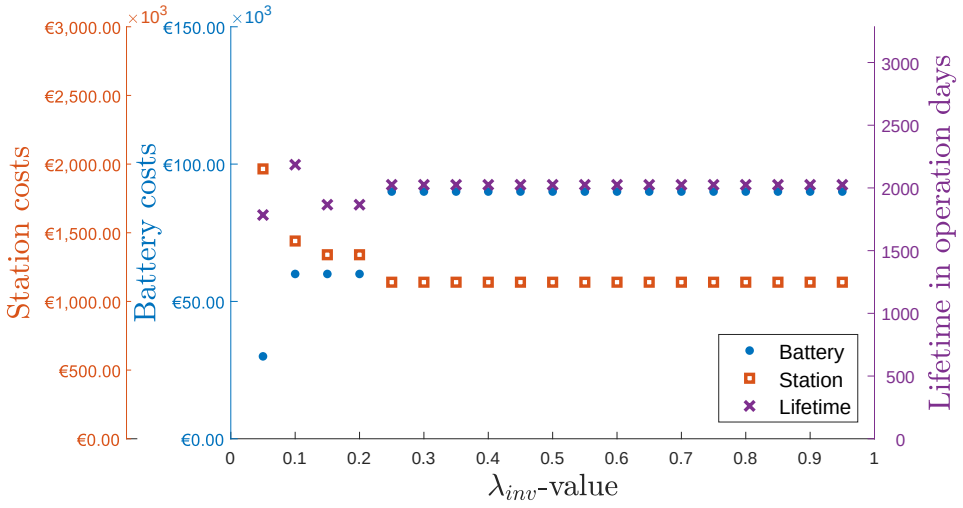

(A) Solutions for $A.1$ model

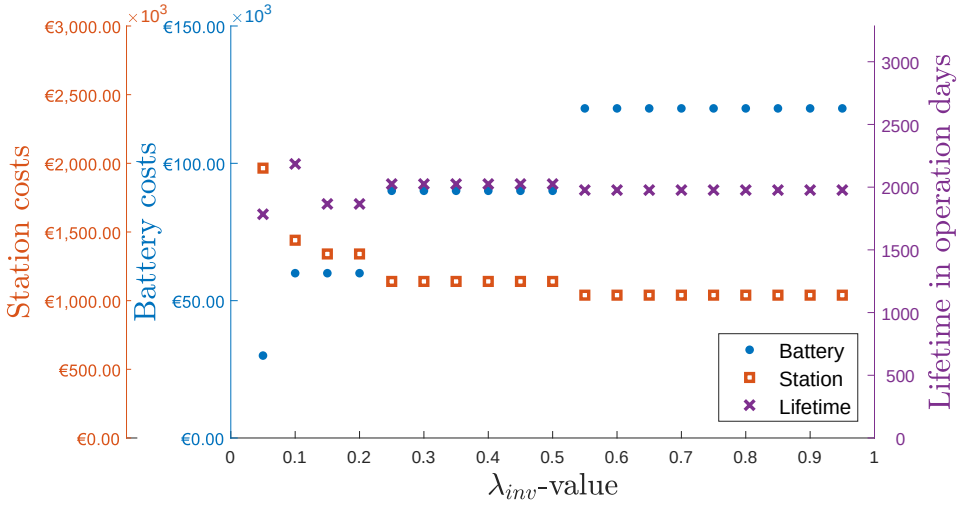

(B) Solutions for $A.2$ model

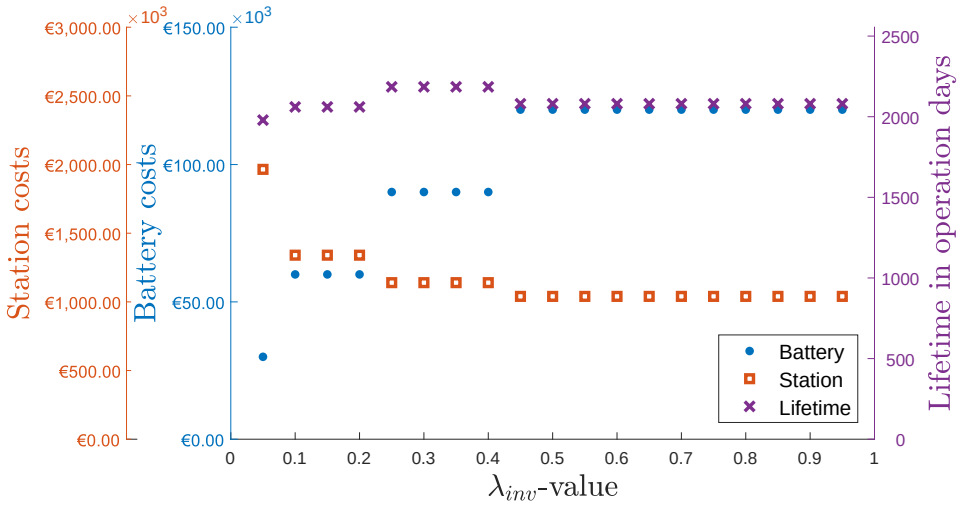

(C) Solutions for $A.3$ model

FIGURE 5.3: *λ-graphs depicting the solutions for various values of λ_{inv}, showing each solution's battery costs, station costs and lifetime per battery*

only interested in cycle lifetime. The actual lifetime in years might deviate from these numbers because of the calendar aging, i.e. the degradation due to storage conditions. For the further interpretation of the results the storage conditions are assumed to be optimal and degradation is fully described by cycle aging.

Some obvious observations that can be made from Figure 5.3 are that the station costs, and thus the number of stations, decrease as the weight of the investment costs in the objective function, λ_{inv} increases. To the contrary, the battery costs increase as λ_{inv} increases. This is caused by a need for larger batteries as fewer stations are installed. Since the total costs of all batteries is significantly less than the costs for installing stations, decreasing the number of stations at the expense of increasing battery sizes is optimal as the weight of investment is increased. This resul is fairly intuitive and as expected.

Larger batteries have the advantage of attaining a larger lifetime in general. If a large battery follows the same charging pattern as a smaller sized battery, daily DOD would be lower as it is relative to the battery size. The induced DOD degradation would be less and as DOD contributes the most to the degradation in total (this is discussed in more detail in Section 5.4) the battery's lifetime will likely increase. The more striking observation to be made here is that total degradation is more or less equal for every value of λ_{inv}. This can be explained by the form of degradation in the objective function. Degradation is expressed as costs, which is directly related to the size of the battery. Decreasing λ_{inv} (and thus increasing λ_{deg}) does therefore not induce an increase in battery life, rather does it maintain a somewhat constant battery lifetime for decreasing battery sizes.

Another observation from Figure 5.3 is the differences between the solutions for $A.1$, $A.2$ and $A.3$. Introducing the possibility of a decrease in energy level with every bus cycle, which is done with the $A.2$ model, allows for a slight decrease in station costs for values of $\lambda_{inv} \geq 0.55$. The bus cycle can now be completed with less recharges on the route and fewer stations need to be installed. This comes at a cost of bigger sized batteries and a slightly higher degradation rate, resulting in higher degradation costs, but the decrease in station costs dominates for larger λ_{inv} weights and the overall objective values improve compared to $A.1$.

Further extending the model by introducing the possibility to have different charging profiles for every bus cycle, which is done with the $A.3$ model, enables the solver to find solutions with fewer stations for values $\lambda_{inv} \geq 0.45$ and improves battery lifetime for solutions with the same number of stations and size of on-board battery.

5.2.2 Results with ε-constraint method

Here the results obtained with the ε-constraint method, i.e. the B.x models, are discussed. Figure 5.4 shows the solutions for various values of ε, similar to the graphs in Figure 5.3. Alongside these graphs a second graph is depicted for all three models. This graph shows the progression of the objective value for the various values of ε and shows the lifetime as is imposed by ε as well as the lifetime that is obtained with the solution.

As expected the objective values increase as the maximum allowed degradation ε decreases. We can see a pattern for decreasing battery degradation. The size of the on-board battery is first increased in order to decrease degradation. Recall that as DOD degradation is the most contributing factor to battery degradation and a larger battery that follows a similar charging pattern will have lower DOD-degradation. After a few increments in battery size it is more efficient to instead increase the

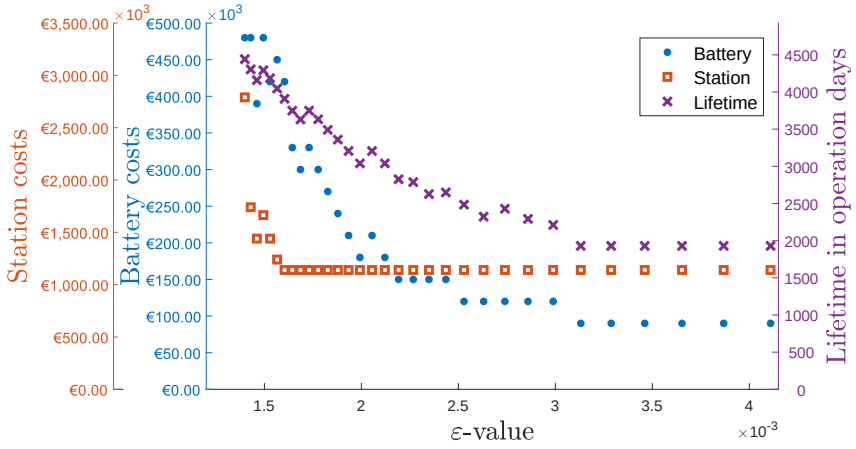

(A) Solutions for $B.1$ model

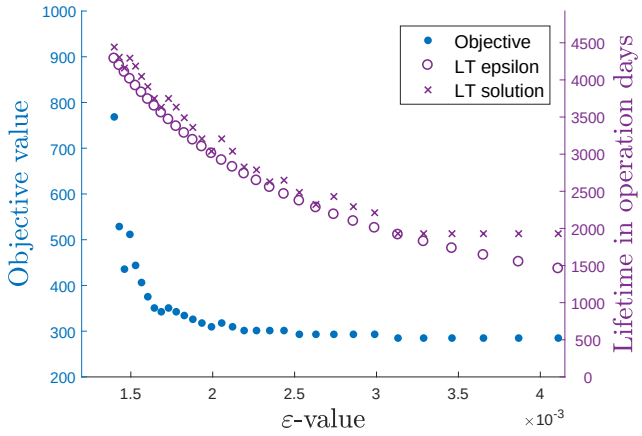

(B) Lifetime compared to ε for $B.1$ model

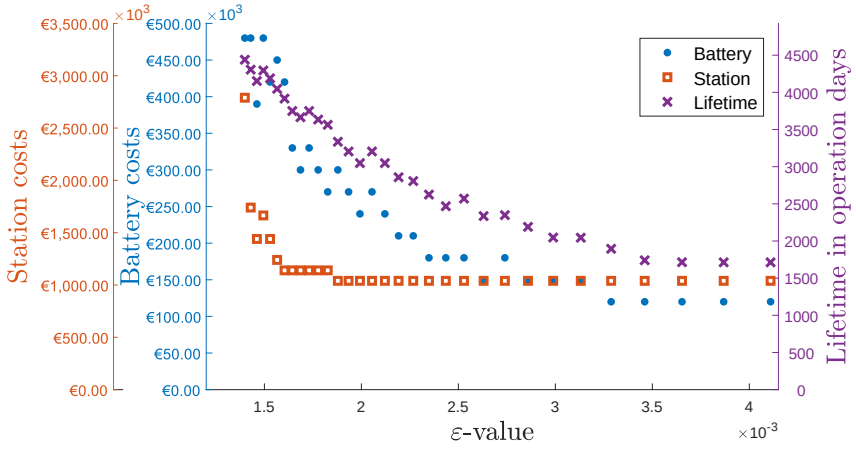

(C) Solutions for $B.2$ model

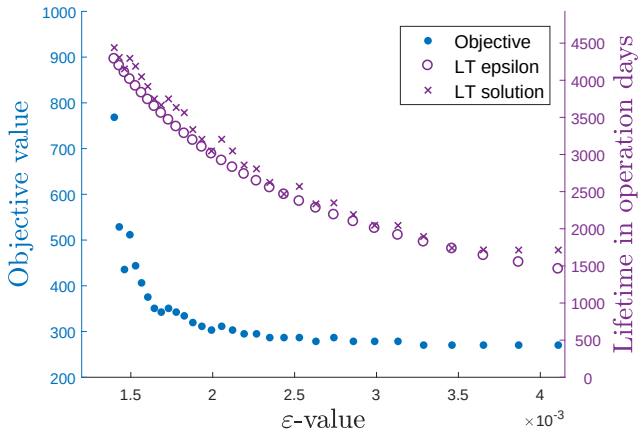

(D) Lifetime compared to ε for $B.2$ model

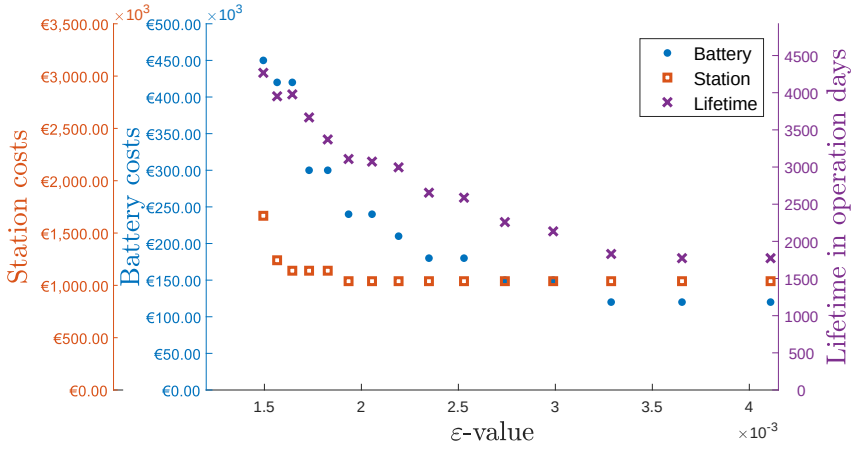

(E) Solutions for $B.3$ model

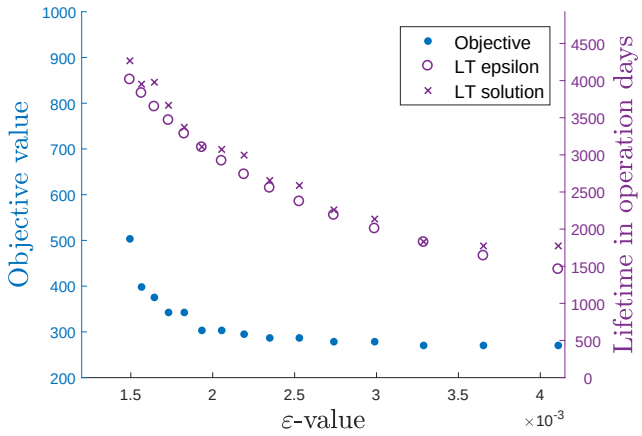

(F) Lifetime compared to ε for $B.3$ model

FIGURE 5.4: *Pareto graphs for ε-constraint method. For each model two graphs are displayed, one depicting the solutions' battery costs, station costs, and lifetime per battery and the other providing insight in the progression of the objective value for decreasing ε-values and the difference between the minimum lifetime imposed by ε and the actual achieved lifetime of the solution*

number of charging stations. The smallest value of ε a solution was found for is 1.4×10^{-3}, corresponding to a battery lifetime of almost 4500 operation days.

Comparing models $B.1$ and $B.2$ we see that the possibility of energy degradation with every bus cycle allows for finding solutions with fewer stations installed for values $\varepsilon \geq 1.85 \times 10^{-3}$. However this comes at a cost of requiring larger on-board batteries, but the overall objective value is improved. For smaller values of ε both models find the same solutions. The $B.3$ model is able to find solutions with the same number of stations as $B.2$ but with smaller on-board batteries for the complete range of values for ε. The problem was solved with $B.3$ for fewer ε values as the required time to find a solution was significantly more. The running time took 50 up to 150 times more time as for solving the $B.1$ and $B.2$ models and the maximum solving time was set at 3600s, which was exceeded once.

Looking at Figures 5.4b, 5.4d and 5.4f the battery lifetime achieved with the solutions often differs from the minimum lifetime that is imposed by ε. This seems counterintuitive, because why was a lower cost solution not found as the ε-constraint is not strictly met? It might exist but is perhaps not found due to the design of the iterative method used to calculate DOD degradation. If in an iteration the used parameters for DOD degradation correspond to a higher DOD than that of the optimal DOD, the degradation of the optimal solution is overestimated and does not satisfy the ε-constraint. Also, if in an iteration the used parameters for DOD degradation correspond to a lower DOD than that of the optimal DOD, a solution might be found that is infeasible after adjusting the DOD degradation. This can probably be improved by increasing the number of values in the list to iterate over.

The results obtained with the '*lin*' method are presented in Figure 5.5 for comparison. Here the lifetime achieved in the solution does not deviate from the lifetime corresponding to the ε-value as much. Furthermore, this method is able to find solutions for even smaller values of ε, as low as 1.24×10^{-3}, corresponding to a lifetime of over 4800 operation days. At first glance this method seems to outperform the iterative method. However, if we adjust the lifetime by correcting the DOD degradation to its true value, the solutions become infeasible for values $\varepsilon < 1.5 \times 10^{-3}$. This exemplifies the severity of lifetime overestimation caused by the deviation of linear approximated DOD degradation to its true value. In this particular case the most severe overestimation was 8.4%, or 373 operation days.

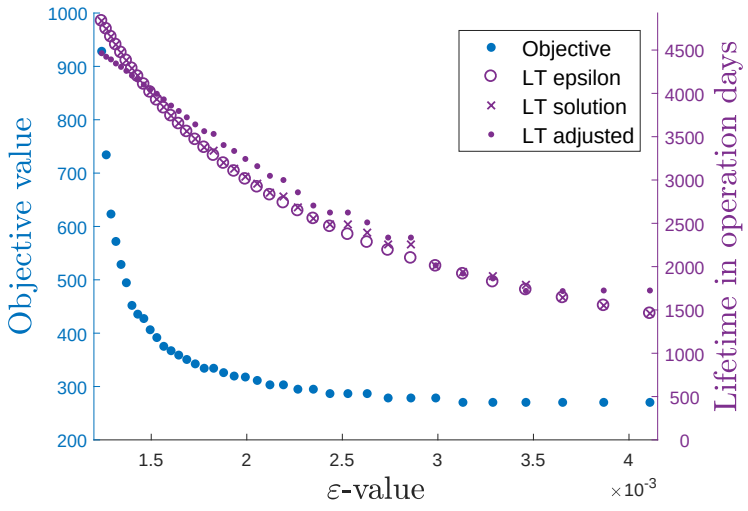

FIGURE 5.5: *Lifetime compared to ε for $B.2$, results obtained with* 'lin'

5.2.3 Evaluation of MOP methods

The two applied MOP solving methods perform differently with regard of the optimization of both objectives. The weighted sum method might be deemed more suitable to serve the problem posed in this research, i.e. optimizing TCO. However, the objective function of the weighted sum method in its current form fails to improve battery lifetime as the weight for the degradation part of the objective increases. This is mainly because the degradation objective is directly related to battery size, consequently preferring solutions with smaller battery size and thus shorter achievable lifetimes. The concept of expressing degradation in costs is ineffective.

The ε-constraint method is better at optimizing battery lifetime but requires a pre-solving decision for the minimum desired lifetime. Setting a minimum requirement for the lifetime might be complicated because the effect on the solution is unknown beforehand. On the other hand, running the model for various values ε would enable planners to choose the solution that fits best to specific requirements.

Given that this problem involves decisions for a long-term period and the planning will have sufficient amount of time (designing an electric bus network tends not to be a critical decision that needs to be made overnight), using the ε-constraint method for this type of problem is preferred over the the weighted sum method in its current form. It is better at exposing the trade-off between the number of stations and battery size and the consequences for the battery lifetime which enable planners to make an informed decision on the balance between network costs and battery lifetime.

5.3 Value of the Model

In order to assess the value of incorporating battery degradation in the charging network design the solutions with and without degradation are summarized in one overview in Table 5.2. Models $O.x$ denote the solutions without degradation, which is similar to Models $A.x$ with parameters $\lambda_{deg} = 0$, $\lambda_{inv} = 1$. These will serve as a benchmark. From this table the different effect of both MOP methods on battery size are accentuated. As the emphasis on battery degradation increases (decreasing λ_{inv} for $A.x$ models, decreasing ε for $B.x$ models) the weighted sum method decreases the battery size whereas the ε-constraint method increases the battery size.

First we compare the solutions of the models with battery degradation to the solution without degradation that possess similar characteristics. Solutions with the same battery size, number of stations and station costs manage to improve battery lifetime. This is summarized in Table 5.3. The improvement for the basic model $X.1$ is only 5% but for the extended models improvements of around 15% and 17% are realized. This shows that integrating battery degradation in the charging network design can lead to significant improvements in battery life, even without an increase in costs, just by being smarter about where to install the charging facilities.

	$X.1$	$X.2$	$X.3$
$O.x$	1931	1722	1785
$A.x$	2025	1977	2080
improvement	94	255	295
% improvement	4.87%	14.81%	16.53%

TABLE 5.3: *Battery lifetime achieved with similar solution characteristics*

Model	Class of solutions	$\lambda_{inv}/\varepsilon$	Battery size	Battery lifetime	# FFS	# SFS	Station costs
O.1		-	15 kWh	1931	6	0	€ 1,140,000
A.1		0.05	5 kWh	1784	10	2	€ 1,965,000
		0.10	10 kWh	2185	8	0	€ 1,440,000
	Same solutions	0.15-0.20	10 kWh	1866	6	0	€ 1,340,000
	Same solutions	0.25-0.95	15 kWh	2025	6	0	€ 1,140,000
B.1	Same station costs, small battery	4.11E-03	15 kWh	1929	6	0	€ 1,140,000
		⋮	⋮	⋮			
		1.88E-03	40 kWh	3360			
	Same station costs, large battery	1.83E-03	45 kWh	3490	6	0	€ 1,140,000
		⋮	⋮	⋮			
		1.60E-03	70 kWh	3909			
	Large battery, increasing station costs	1.57E-03	75 kWh	4047	6	0	€ 1,240,000
		⋮	⋮	⋮	⋮		⋮
		1.43E-03	80 kWh	4305	10		€ 1,740,000
		1.40E-03	80 kWh	4442	16	1	€ 2,790,000
O.2		-	20 kWh	1722	5	0	€ 1,040,000
A.2		0.05	5 kWh	1784	10	2	€ 1,965,000
		0.10	10 kWh	2185	8	0	€ 1,440,000
	Same solutions	0.15-0.20	10 kWh	1866	6	0	€ 1,340,000
	Same solutions	0.25-0.50	15 kWh	2025	6	0	€ 1,140,000
	Same solutions	0.55-0.95	20 kWh	1977	5	0	€ 1,040,000
B.2	Same station costs, small battery	4.11E-03	20 kWh	1713	5	0	€ 1,040,000
		⋮	⋮	⋮			
		1.88E-03	50 kWh	3335			
	Same station costs, large battery	1.83E-03	45 kWh	3564	6	0	€ 1,140,000
		⋮	⋮	⋮			
		1.60E-03	70 kWh	3916			
	Large battery, increasing station costs	1.57E-03	75 kWh	4047	6	0	€ 1,240,000
		⋮	⋮	⋮	⋮		⋮
		1.43E-03	80 kWh	4306	10		€ 1,740,000
		1.40E-03	80 kWh	4439	15	1	€ 2,790,000
O.3		-	20 kWh	1785	5	0	€ 1,040,000
A.3		0.05	5 kWh	1979	10	2	€ 1,965,000
	Same solutions	0.10-0.20	10 kWh	2061	6	0	€ 1,340,000
	Same solutions	0.25-0.40	15 kWh	2185	6	0	€ 1,140,000
	Same solutions	0.45-0.95	20 kWh	2080	5	0	€ 1,040,000
B.3	Same station costs, small battery	4.11E-03	20 kWh	1774	5	0	€ 1,040,000
		⋮	⋮	⋮			
		1.93E-03	40 kWh	3108			
	Same station costs, large battery	1.83E-03	50 kWh	3371	6	0	€ 1,140,000
		⋮	⋮	⋮			
		1.64E-03	70 kWh	3978			
		1.57E-03	70 kWh	3952	6	0	€ 1,240,000
		1.49E-03	75 kWh	4267	10	0	€ 1,740,000

TABLE 5.2: *An overview of the solutions compared to the solutions without integrated battery degradation. Solutions with similar characteristics are grouped together and for non-similar characteristics the range of occurring values is given. The column 'Class of solutions' defines their connection.*

		X.1	*X*.2	*X*.3
O.x	Battery size	15kWh	20kWh	20kWh
benchmark	Lifetime	1931	1722	1785
B.x	Battery size	×1.7 (*25kWh*)	×1.5 (*30kWh*)	×1.5 (*30kWh*)
increase in:	Lifetime	46.39% (*2827*)	52.41% (*2625*)	48.73% (*2655*)
B.x	Battery size	×2.3 (*35kWh*)	×2.5 (*50kWh*)	×2.0 (*40kWh*)
increase in:	Lifetime	66.08% (*3207*)	93.67% (*3335*)	74.12% (*3108*)
B.x	Battery size	×5.0 (*75kWh*)	×2.8 (*55kWh*)	×2.5 (*50kWh*)
increase in:	Station costs	8.77%	9.62%	9.62%
	Lifetime	109.58% (*4047*)	117.73% (*3749*)	105.45% (*3667*)

TABLE 5.4: *Achieved improvements in battery lifetime when larger batteries are installed. Three solutions are presented for every model. The increase in costs, battery size and battery lifetime is compared to the benchmark of the O.x model. The increase in station costs is 0% for the solutions where it is omitted.*

Next we look at the achieved improvements in battery life for similar station costs but with larger batteries. This is depicted in Table 5.4. For every model three solutions are presented; one with a slightly larger battery size (less than 2× the battery size in the benchmark solution), another with an even larger battery size (more than 2×) and a third with slightly higher station costs (one extra station installed). This shows that if battery size is increased by roughly 50%, its lifetime will increase by around 50% as well. However, the increase in battery life does not follow the increase in battery size exactly. More than doubling the battery size causes the battery life to increase with roughly 66-94% and combining that with an installment of an extra station ups the improvement only to 105-118%. Nevertheless, these can be cost efficient solutions compared to the benchmark, depending on the costs for stations and the marginal costs of increasing the fleet's battery size.

In this model the increase in battery costs is directly linearly related to its size and in that case choosing a larger battery might not be cost efficient financially if the increase in lifetime is proportional to the increase in size and therefore in costs. There is no gain in costs per operated time unit and most financial departments will try to postpone capital investments to the latest possible moment. However, this financial viewpoint does not include the extra replacements necessary with shorter battery lifetimes, which induce extra maintenance costs and have a larger environmental impact because of chemical waste, or the higher uncertainty due to more frequent defects, affecting service rates and inducing 'down-time' costs. Especially in the public sector aspects that affect the good-will under its users, such as service rates, are generally more important. Choosing larger battery sizes with longer lifetimes can in that case therefore be cost efficient as well. Moreover, it is likely that battery costs will not be exactly linear in size, but that the average costs per kWh will decrease as total size increases.

Furthermore, the added costs of installing one extra station probably cannot compete with the benefits of longer battery lifetime for the fleet of a single-line network. However, for a multiple-line network, installing an extra charging facility at a stop that is serviced by several bus lines has an effect on a larger fleet and has a better potential of being cost efficient.

5.3.1 Added value of charging policy optimization

The *X*.3 models manage to find solutions that slightly improve the battery lifetime with smaller battery sizes for equal station costs. However, the required time to obtain these solutions is disproportonially larger than for *X*.2 models, whilst the solutions are equal in terms of where charging stations are installed. It is therefore recommended that the extra charging pattern optimization is not incorporated in

the network design model. Rather the network is designed with a model that incorporates battery degradation and afterwards the charging policy can be optimized. The charging optimization could even decrease battery costs without decreasing the battery lifetime, as we saw from the results in Figure 5.4.

5.4 Degradation Factors

With the used parameters the contribution of the three different degradation factors DOD, SOC and temperature was on average 56.6%, 43.3% and 0.1% resp. to the total degradation. Temperature seems to be rather unimportant with regard to cycle aging, as was predicted in Chapter 3. The other two factors have similar contributions to the total degradation, but in most cases DOD degradation had a larger contribution. The parameters of the degradation functions cause to prioritize reducing DOD degradation over reducing SOC degradation, i.e. preferring small DOD over low average SOC. A lower DOD generally coincides with a higher average SOC and vice versa. Since the goal was to build an universal model it is necessary to analyze the sensitivity of solutions to these parameters as the degradation parameters are likely to be different for different types and brands of battery.

In order to analyze this sensitivity the following approach was used. The degradation functions of DOD and SOC were multiplied with respective multipliers λ_{DOD} and λ_{SOC}. These multipliers were adjusted to give more or less weight to their corresponding degradation factor, maintaining the sum to be equal to 2 with benchmark $\lambda_{SOC} = \lambda_{DOD} = 1$. In Table 5.5 the solutions for one instance of $B.2$ model for various ratios of $\lambda_{SOC}/\lambda_{DOD}$ exemplifies the changes. As can be expected the average SOC decreases and DOD increases as the ratio increases. The battery lifetime is approximately constant because it is restricted by the ε-constraint. We see that the station costs are constant as well, but battery size decreases.

However, caution needs to be taken when drawing conclusions from these numbers because this approach of analysis affects the absolute value of both degradation factors as well. Especially comparing solutions obtained with the ε-constraint method is problematic since the absolute value of degradation is what is restricted by ε. We cannot simply conclude that batteries with technologies that are more vulnerable to SOC degradation tend to need smaller batteries to achieve the same result, compared to batteries less vulnerable to SOC degradation. Nevertheless it does show that the relative contribution of the different degradation factors can significantly affect the optimal solution. An example of this is shown in Figure 5.6, where more weight on the SOC degradation induces not only a smaller battery but a charging profile with more (relative) energy depletion over the day opposed to little depletion at high average energy level.

Ratio $\lambda_{SOC}/\lambda_{DOD}$	**1**	**2**	**3**	**4**
Battery size	45	40	30	20
Lifetime	3243.1	3138.8	3077.9	3010.3
Station costs	€ 1,040,000	€ 1,040,000	€ 1,040,000	€ 1,040,000
DOD	0.372	0.396	0.494	0.800
SOC	0.805	0.795	0.755	0.620

TABLE 5.5: *Different solutions when weight of SOC degradation is increased for $B.2$ with $\varepsilon = 0.00205$*

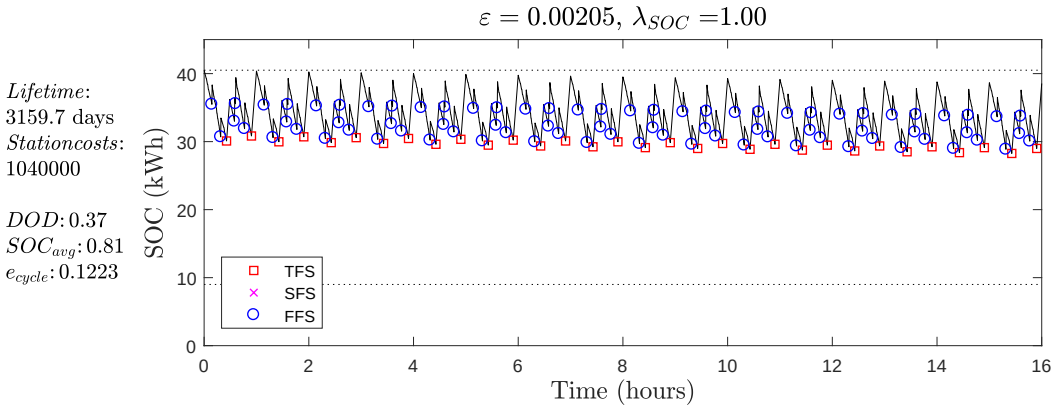

(A) $\lambda_{SOC}/\lambda_{DOD} = 1$

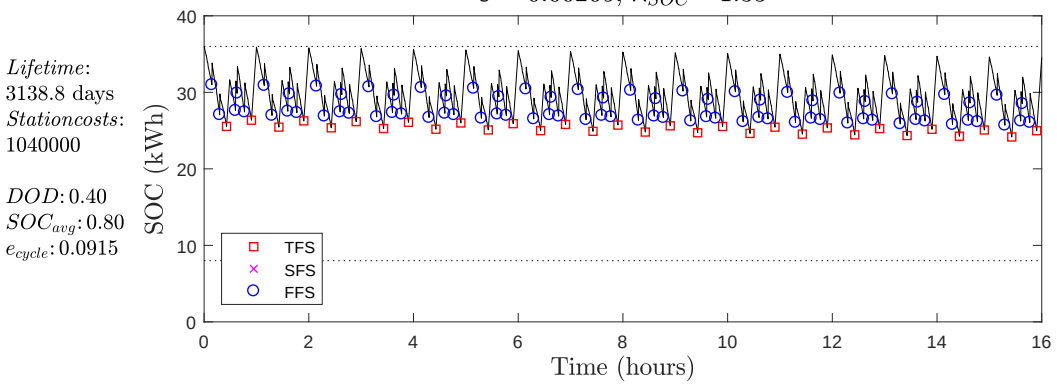

(B) $\lambda_{SOC}/\lambda_{DOD} = 2$

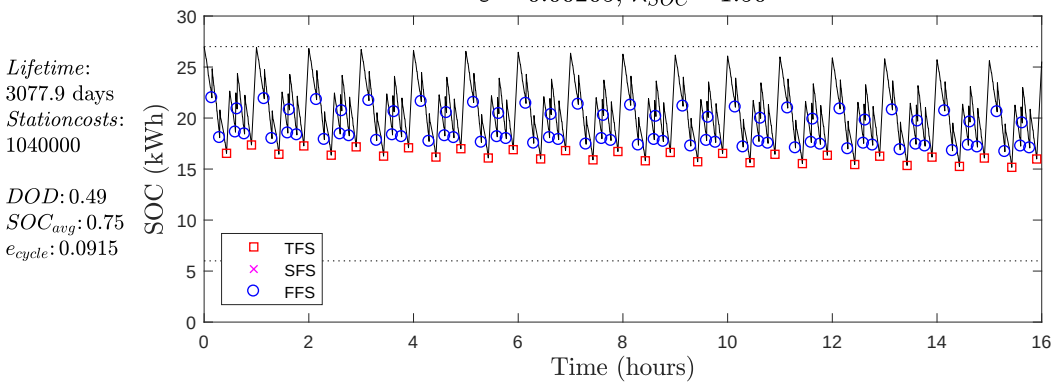

(C) $\lambda_{SOC}/\lambda_{DOD} = 3$

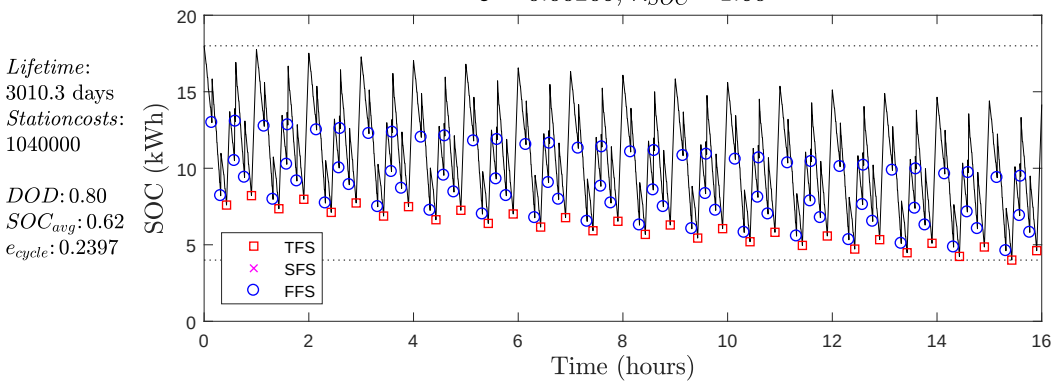

(D) $\lambda_{SOC}/\lambda_{DOD} = 4$

FIGURE 5.6: *Energy graphs for solutions obtained with B.2 model, $\varepsilon = 0.00205$, for different ratios $\lambda_{SOC}/\lambda_{DOD}$*

Chapter 6

Conclusion and Further Research

In this Chapter the drawn conclusions are summarized in Section 6.1. The discussion can be found in Section 6.2 and suggestions for further research in Section 6.3.

6.1 Conclusion

The aim of this research was to find a way to incorporate battery degradation in a charging facility location problem in order to improve accuracy in TCO optimization. This involved combining two objectives in one MILP, also known as a MOP. Various methods exist for solving MOPs and two of those were applied to this problem, the weighted sum and ε-constraint methods, presented as models $A.1$ and $B.1$ in Chapter 3. The solution space of the problem was broadened to better approximate reality, first by adding the option of energy depletion with every buscycle ($X.2$), and even further by also freeing the charging policy from the requirement to be equal for every buscycle ($X.3$). The models were tested with semi-realistic data that was synthesized based on data from a bus line operated in Rotterdam.

In Chapter 5 the results obtained with the various models were presented and compared. Although weighted sum method might be the more intuitive approach for TCO optimization, it failed to effectively increase the lifetime of on-board batteries. The ε-constraint method proved better in revealing the trade-off between battery lifetime and investment costs and is therefore more appropriate for this problem. Especially considering that with planning an electric bus network there is enough time to solve the problem to optimality for varying ε values, it makes more sense to use the ε-constraint approach to make an informed decision on the size of on-board batteries and how to achieve a cost efficient network design.

For the case study of this research the incorporation of battery degradation in the charging facility location problem improves the battery life even without increasing the battery size or the number of stations installed. This alone shows the added value of this model compared to facility location problems without an incorporated battery degradation model, as it provides a 'smarter' network design with the same number of stations. For this case the battery lifetime increased further with approximately the same rate as for increasing the battery size. Although these results might be very case-specific, they are promising for the goal of improving battery lifetime.

The proposed extensions for the model performed differently regarding solvability and solution quality. Where the $X.2$ models are able to find better solutions with regard to battery lifetime, battery size and the location of stations in approximately the same amount of time, the $X.3$ models only improved those solutions slightly further in significantly more time. For the case studied in this research a different solution in terms of charging facility placement was never found. It is therefore recommended to solve this problem with the extension of energy depletion, but improving the charging policy per bus cycle afterwards.

6.2 Discussion

During this research some issues arose that affect the validity of this model. These issues are addressed here and some ideas for improvement are discussed here.

Some of the issues regard the battery degradation model. Firstly, the used parameters were obtained from literature and might differ significantly for various cases. This is easily adjusted in the model obviously, but drawn conclusions might prove incorrect for other types of battery (such as the temperature degradation being insignificant). Since the model is aimed to be universal, it should be tested on various battery technological configurations and their respective degradation parameters. This requires data from different battery manufacturers, which was not available for this research. The degradation parameter sensitivity analysis was conceived to research the validity of the drawn conclusions, but it is difficult to isolate individual effects. This sensitivity analysis can be improved by using realistic bounds on the parameters and comparing the solutions for various combinations of parameters. This again requires data from different battery manufacturers, which was unavailable.

Moreover, it is assumed that the battery degradation model is able to describe degradation for all battery technologies. However, most relations between degradation and operation were obtained from literature specifically for Lithium-ion batteries. It is unknown if other contributing factors are involved for other technologies. However, as long as a linear relation exists or can be approximated, it is easily added to the model. This accentuates another potential weakness: the battery degradation model being oversimplified. In reality it is a rather complex phenomenon and the current linear approximation might not do it justice, diverging too far from reality. Although simplicity is a requirement for this model, further tuning, e.g. with help of advanced simulation models such as NREL, is necessary.

Furthermore, the incorporation of DOD degradation had its flaws. The iterative method is not optimal, neither is the linear approximation method. The iterative method might be improved by going over a larger list of DOD values, which would increase solving speed. A better solution would be to improve the linear approximation of the DOD degradation such that the deviation from the true degradation would be minimal, but this requires further research.

Lastly, since the battery size is involved in both the investment objective and the degradation objective it is harder to achieve the goal of battery life optimization with the weighted sum method. This was necessary because the concept of degradation costs was adopted to incorporate degradation. Dropping this concept might improve the performance of the weighted sum method. However, this requires transforming one or both objectives such that they have comparable values.

6.3 Further research

Although the model provides useful insights and has the potential of increasing accuracy of TCO estimation for EB networks, it has its limitations. To further advance the field of electric public transport some suggestions:

The first obvious next step is to upscale the model to design a network for multiple bus lines. A complete network has the potential advantage of installing charging stations on crosspoints of bus lines and dispersing investment costs over multiple operations. One rather simple idea is to identify these crosspoints as 'loading hubs' with lower installment costs for loading stations, depending on the number of lines that the hub services. Then optimize bus lines separately with the current model and

combine solutions of different lines to a complete network. The disadvantage of this approach could be that the solutions of different bus lines create line-specific fleets, obstructing the possibility of sharing rolling stock between different operations. This might be solved by imposing extra restrictions in the model. Another approach is to model the complete network and optimize the charging infrastructure simultaneously for all bus lines (e.g. Kunith, Mendelevitch, and Goehlich, 2017). Extending this model with integrated battery degradation is likely to complicate the model significantly, as the total fleet in the solution can be heterogeneous.

Secondly, the accuracy of battery lifetime/degradation estimation with linear functions needs to be studied, hopefully improving this accuracy for the involved degradation factors. Perhaps a single linear function that is sufficiently accurate can be found for DOD degradation, discarding the need for the iterative method and improving the solutions and solving speed of the model.

Another suggestion to improve TCO is to take into account the schedule and bus stop network. This research showed that the operation decisions have impact on the TCO via the battery degradation and rescheduling or rerouting the existing bus lines might benefit battery lifetime. In the case of a multi-line network this could also decrease the number of stations or the required charging power or size of ESS, which reduces the investment costs. Scheduling models for conventional bus networks seem to be insufficient for application in EB networks because waiting times can vary due to varying charging needs (Kameda and Mukai, 2011; Chao and Xiaohong, 2013; Korsesthakarn and Sripakagorn, 2014).

Furthermore, the model could be improved by incorporating more accurate battery behavior models, such as better approximations of non-linear charging and discharging behavior (Montoya et al., 2017). The battery lifetime could be further improved with help of recharging optimization models for a given, predefined network of charging opportunities, regarding the stress on the electrical grid of simultaneous charging as well (Sweda, Dolinskaya, and Klabjan, 2017). In addition the configuration of the charging facilities could be introduced as decision variable to facilitate optimal recharging policies.

The last suggestion for further research is to efficiently incorporate uncertainties of energy consumption and travel/dwell times in the network design. This can be modeled by means of stochasticity or robust analysis, such as budget of uncertainty, although this decreases the size of the problem that can be solved in an acceptable amount of time significantly (Wehres et al., 2016). Another idea is to make use of dynamic modeling for the charging decisions.

Appendix A

Average SOC

Here the auxiliary variables, or h-variables, used to calculate the average SOC are explained in more detail. Two types of h-variable were introduced, h_{dwell} and h_{travel}. Both describe the area under the energy level graph over time, h_{dwell} denotes the graph area for time spent at a stop and h_{travel} during traveltime between two stops. The models contain four constraints calculating these variables, (3.29)-(3.32) in problem $(\mathcal{P}_{A.1})$, and their derivation is shown in this Appendix.

Variable $h_{dwell,s}$ The energy level in the battery upon arrival at the bus stop (z_s), the battery level at departure (w_s) and the time spent at the stop (δ_s) are required to determine the area underneath the energy level graph during dwell time. Since every bus cycle is repeated ρ times, the same area appears ρ times as well under the graph. Therefore a factor ρ is added to the expression. This is not the case for $X.3$ models, where every revisit of a stop is modeled with a separate node. This results in the following expressions for the three different choices for modeling an operation day.

$$
\begin{aligned}
&(\mathcal{P}_{X.1}): && h_{dwell,s} = \tfrac{1}{2}\rho(z_s + w_s)\cdot\delta_s \\
&(\mathcal{P}_{X.2}): && h_{dwell,s} = \tfrac{1}{2}\rho(z_s + w_s)\cdot\delta_s \\
&(\mathcal{P}_{X.3}): && h_{dwell,s} = \tfrac{1}{2}(z_s + w_s)\cdot\delta_s
\end{aligned}
$$

Variable $h_{dwell,1}$ The area under the graph during charging at the depot is a little different and is included in the auxiliary variable for stop 1 ($h_{dwell,1}$). The area under the graph during charging at this terminal stop is included in the auxiliary variable at the last stop ($h_{dwell,A}$). Note that stop 1 and stop A are physically the same stop, denoting the starting and ending point of the bus cycle. The energy level in the on-board battery upon arrival at the depot is equal to the energy level at the end of an operation day minus the energy required to reach the depot from the last stop ($w_A - \nu_A$). The battery is assumed to be linearly recharged up to 100% of its capacity at the lowest possible power and thus utilizing the available time (δ_{depot}) for recharge fully. For $X.2$ models the ending energy level needs to be corrected for the decline in energy over the day. This results in the following expressions.

$$
\begin{aligned}
&(\mathcal{P}_{X.1}): && h_{dwell,1} = \tfrac{1}{2}(\textstyle\sum_{i\in I} b_i\cdot\kappa_i + w_A - \nu_A)\cdot\delta_{depot} \\
&(\mathcal{P}_{X.2}): && h_{dwell,1} = \tfrac{1}{2}(\textstyle\sum_{i\in I} b_i\cdot\kappa_i + w_A - (\rho-1)e_{cycle} - \nu_A)\cdot\delta_{depot} \\
&(\mathcal{P}_{X.3}): && h_{dwell,1} = \tfrac{1}{2}(\textstyle\sum_{i\in I} b_i\cdot\kappa_i + w_A - \nu_A)\cdot\delta_{depot}
\end{aligned}
$$

Variable $h_{travel,s}$ Similar to the $h_{dwell,s}$ variable, to determine the area underneath the energy level graph during travel the required data are the energy level in the battery when leaving a stop (w_s), the battery level upon arriving at the next stop (z_{s+1}) and the traveltime (τ_s). As the bus cycle is repeated ρ times, a factor ρ is added, except for X.3 models.

$$
\begin{aligned}
(\mathcal{P}_{\text{X.1}}): &\qquad h_{travel,s} = \tfrac{1}{2}\rho(w_s + z_{s+1}) \cdot \tau_s \\
(\mathcal{P}_{\text{X.2}}): &\qquad h_{travel,s} = \tfrac{1}{2}\rho(w_s + z_{s+1}) \cdot \tau_s \\
(\mathcal{P}_{\text{X.3}}): &\qquad h_{travel,s} = \tfrac{1}{2}(w_s + z_{s+1}) \cdot \tau_s
\end{aligned}
$$

Variable $h_{travel,A}$ The area under the energy level graph for traveling from and to the depot at the start and end of an operation day is denoted by the auxiliary variable for the last stop ($h_{travel,A}$). When calculating the area for travel from and to the depot the required information is captured in the variables denoting energy level at the end of the bus cycle (w_A), energy required to travel from the first stop to the depot and from the last stop to the depot (ν_1 and ν_A) and the traveltime (τ_{depot}). As mentioned before, the battery level is assumed to be recharged up to 100% of its capacity. Using that $\nu_1 = \nu_A$ we can simplify the expression as follows.

$$
\begin{aligned}
h_{travel_A} = &\quad \tfrac{1}{2}(\textstyle\sum_{i\in I} b_i \cdot \kappa_i + \sum_{i\in I} b_i \cdot \kappa_i - \nu_1) \cdot \tau_{depot} + \tfrac{1}{2}(w_A + w_A - \nu_A) \cdot \tau_{depot} \\
= &\quad (\textstyle\sum_{i\in I} b_i \cdot \kappa_i + w_A - \nu_A) \cdot \tau_{depot}
\end{aligned}
$$

For X.2 models the ending energy level needs to be corrected for the decline in energy over the day. The expressions for the three different models are as follows.

$$
\begin{aligned}
(\mathcal{P}_{\text{X.1}}): &\qquad h_{travel,A} = (\textstyle\sum_{i\in I} b_i \cdot \kappa_i + w_A - \nu_A) \cdot \tau_{depot} \\
(\mathcal{P}_{\text{X.2}}): &\qquad h_{travel,A} = (\textstyle\sum_{i\in I} b_i \cdot \kappa_i + w_A - (\rho - 1)e_{cycle} - \nu_A) \cdot \tau_{depot} \\
(\mathcal{P}_{\text{X.3}}): &\qquad h_{travel,A} = (\textstyle\sum_{i\in I} b_i \cdot \kappa_i + w_A - \nu_A) \cdot \tau_{depot}
\end{aligned}
$$

average SOC The sum over all the h-variables is equal to the total area under the energy level graph for a full day (24 hours). To express this in relative energy level, or state of charge, this sum is divided by the battery capacity and to calculate the average over time this value is then divided by the duration of one day in seconds. However, since the size of the on-board battery is chosen from a set of values and multiplication of variables is impossible due to the linearity principle of MILPs, separate variables for average SOC were introduced for every possible battery size. This poses no problem as long as the SOC_j-variable corresponding to the chosen battery size captures the true average SOC and all other SOC_i-variables take on value 0. The following expression was obtained to meet that requirement.

$$
b_i - SOC_{avg,i} \leq \frac{\sum_{j\in I} b_j \cdot \kappa_j}{\kappa_i} - \frac{\sum_{s\in S} \left[h_{dwell,s} + h_{travel,s}\right]}{\kappa_i \cdot \theta_{day}} \qquad \forall i \in I
$$

For the battery size k that is chosen in the solution the first term in the left-hand side of the expression is equal to 1, as is the first term in the right-hand side of the expression. The second term in the right-hand side of the expression is equal to the average SOC and since the objective function is increasing in the value for $SOC_{avg,k}$,

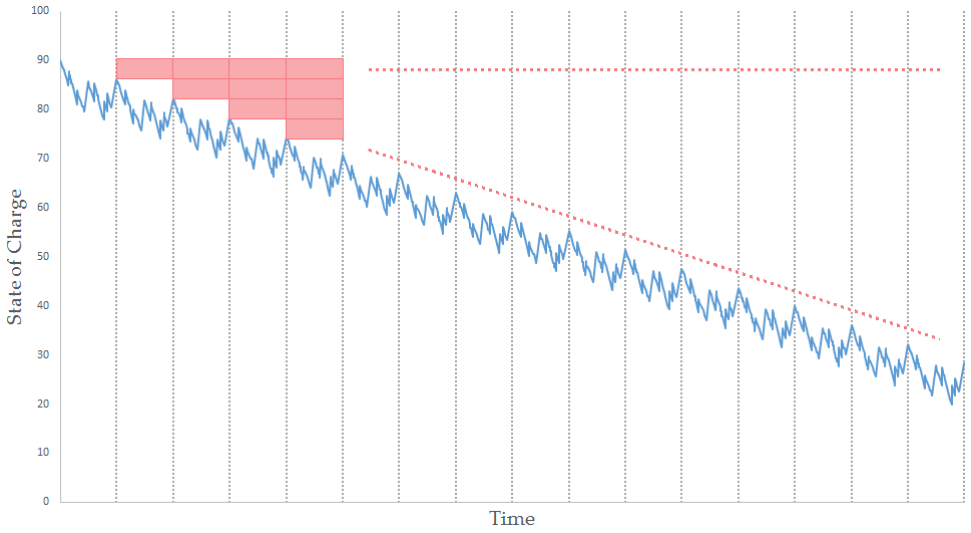

FIGURE A.1: *For X.2 models the sum of the h-variables needs to be corrected for the decline in energy defined by e_{cycle}. The gray vertical lines indicate separate bus cycles, the red areas indicate the excess in the sum*

it's value will be set to the lowest value possible satisfying the inequality, which is the value of the average SOC. For battery sizes l not chosen in the solution the first term of the left-hand side is equal to 0. In order to satisfy that the right-hand side is never less than 0 (otherwise we need $SOC_{avg,l} > 0$ to satisfy the inequality), the first term of the right-hand side is set to be the ratio of the chosen battery size k to battery size l. This ratio will always be larger than the second term of the right-hand side, since it corresponds to the value it will assume when the sum of the h-variables is as large as possible for the chosen battery size k. Again, the value for $SOC_{avg,l}$ is set to the lowest possible value satisfying the inequality, which is 0.

For $X.2$ models the sum of h-variables needs to be adjusted for the possible decline in energy level with every buscycle. Without adjustment the sum would be equal to ρ times the area under the first bus cycle. However, the other $(\rho - 1)$ buscycles correspond to a smaller area than their predecessor. To be exact, each buscycle's area diminishes with an area of $e_{cycle} \times \theta_{cycle}$, i.e. the product of the loss in energy over one buscycle and the duration of one buscycle. This is visualized in Figure A.1. The sum of these excess areas must be subtracted from the sum of h-variables. The total excess can be expressed as

$$(1 + 2 + 3 + \ldots + \rho - 1)\theta_{cycle}e_{cycle} = \tfrac{1}{2}(\rho^2 - \rho)\theta_{cycle}e_{cycle}.$$

This results in the following constraint for the average SOC.

$$b_i - SOC_{avg,i} \leq \frac{\sum_{j \in I} b_j \cdot \kappa_j}{\kappa_i} - \frac{\sum_{s \in S} \left[h_{dwell,s} + h_{travel,s}\right] - \frac{1}{2}(\rho^2 - \rho)\theta_{cycle}e_{cycle}}{\kappa_i \cdot \theta_{day}} \quad \forall i \in I$$

Appendix B

Extended Models

The models with extensions for decrease in energy level after every buscycle and optimization of charging profile are printed here in full.

Extension for energy depletion per bus cycle The X.2 models are formulated as follows, where the blue highlighted parts correspond only to the model with weighted sum method and the green highlighted parts to the model with the ε-constraint method.

$$\min \quad \lambda_{inv}\left(\beta \sum_{i\in I} \frac{\Gamma_{batt,i}\cdot b_i}{\eta_{batt,i}} + \sum_{t\in T}\left[\frac{\sum_{s\in S} x_s^t\cdot \Gamma_s^t + \sum_{d\in D} x_d^t\cdot \alpha_d^t}{\eta^t}\right]\right) + \lambda_{deg}\cdot\beta\cdot g_{deg}^{\lambda}(DOD, SOC_{avg}, b)$$

s.t

$$
\begin{array}{rcll}
\varepsilon_{deg} & \geq & \beta\cdot g_{deg}^{\varepsilon}(DOD, SOC_{avg}, x) & , \\
z_s & = & w_{s-1} - \mu_{s-1} & \forall s\in S\backslash\{1\}, \\
z_s & \geq & \sum_{i\in I} b_i\cdot\kappa_i\cdot\zeta + (\rho-1)\cdot e_{cycle} & \forall s\in S, \\
y_s & \leq & \sum_{t\in T} x_s^t\cdot\phi_s^t & \forall s\in S, \\
y_s & \leq & \sum_{t\in T} x_s^t\cdot\delta_s\cdot\pi_s^t & \forall s\in S, \\
w_1 & = & \sum_{i\in I} b_i\cdot\kappa_i\cdot\omega & , \\
w_s & = & z_s + y_s & \forall s\in S, \\
w_s & \leq & \sum_{i\in I} b_i\cdot\kappa_i\cdot\omega & \forall s\in S, \\
w_s & \geq & \sum_{i\in I} b_i\cdot\kappa_i\cdot\zeta + \nu_s + (\rho-1)\cdot e_{cycle} & \forall s\in S, \\
e_{cycle} & = & w_1 - w_A & , \\
v & \leq & z_s - (\rho-1)\cdot e_{cycle} & \forall s\in S, \\
\sum_{i\in I} b_i & = & 1 & , \\
\sum_{t\in T} x_s^t & \leq & 1 & \forall s\in S, \\
x_s^{TFS} & = & 1 & \forall s\in S^{TFS}, \\
x_s^{TFS} & = & 0 & \forall s\in S\backslash S^{TFS}, \\
x_d^t & \leq & \frac{1}{2}\sum_{s\in S_d} x_s^t & \forall t\in T, \forall d\in D, \\
h_{dwell,1} & = & \frac{1}{2}(\sum_{i\in I} b_i\cdot\kappa_i + w_A - (\rho-1)e_{cycle} - \nu_A)\cdot\delta_{depot} & , \\
h_{dwell,s} & = & \frac{1}{2}\rho(z_s + w_s)\cdot\delta_s & \forall s\in S\backslash\{1\}, \\
h_{travel,s} & = & \frac{1}{2}\rho(w_s + z_{s+1})\cdot\tau_s & \forall s\in S\backslash\{A\},
\end{array}
\qquad (\mathcal{P}_{X.2})
$$

$$
\begin{aligned}
h_{travel,A} &= (\textstyle\sum_{i\in I} b_i \cdot \kappa_i + w_A - (\rho-1)e_{cycle} - \nu_A)\cdot \tau_{depot} && ,\\
DOD_i &\geq b_i - \frac{v}{\kappa_i} && \forall i \in I,\\
b_i - SOC_{avg,i} &\leq \frac{\sum_{j\in I} b_j \cdot \kappa_j}{\kappa_i} - \frac{\sum_{s\in S}\left[h_{dwell,s} + h_{travel,s}\right] - \frac{1}{2}(\rho^2-\rho)\theta_{cycle}e_{cycle}}{\kappa_i \cdot \theta_{day}} && \forall i \in I,\\
x_s^t &\in \{0,1\} && \forall t \in T, \forall s \in S,\\
x_d^t &\in \{0,1\} && \forall t \in T, \forall d \in D,\\
b_i &\in \{0,1\} && \forall i \in I,\\
(\mathcal{P}_{\text{X.2}}) \qquad y_s &\geq 0 && \forall s \in S,\\
z_s &\geq 0 && \forall s \in S,\\
w_s &\geq 0 && \forall s \in S,\\
v &\geq 0 && ,\\
e_{cycle} &\geq 0 && ,\\
h_{j,s} &\geq 0 && \forall j \in \{dwell, travel\}, \forall s \in S,\\
DOD_i &\geq 0 && \forall i \in I,\\
SOC_{avg,i} &\geq 0 && \forall i \in I.
\end{aligned}
$$

Extension for optimizing charging policy The X.3 models are formulated as follows, where the blue highlighted parts correspond only to the model with weighted sum method and the green highlighted parts to the model with the ε-constraint method.

$$
\min \quad \lambda_{inv}\left(\beta \sum_{i\in I} \frac{\Gamma_{batt,i}\cdot b_i}{\eta_{batt,i}} + \sum_{t\in T}\left[\frac{\sum_{s\in S} x_s^t \cdot \Gamma_s^t + \sum_{d\in D} x_d^t \cdot \alpha_d^t}{\eta^t}\right]\right) + \lambda_{deg}\cdot\beta\cdot g_{deg}^{\lambda}(DOD, SOC_{avg}, b)
$$

$$
\begin{aligned}
\text{s.t} \qquad \varepsilon_{deg} &\geq \beta \cdot g_{deg}^{\varepsilon}(DOD, SOC_{avg}, x) && ,\\
z_s &= w_{s-1} - \mu_{s-1} && \forall s \in S\backslash\{1\},\\
z_s &\geq \textstyle\sum_{i\in I} b_i \cdot \kappa_i \cdot \zeta && \forall s \in S,\\
y_s &\leq \textstyle\sum_{t\in T} x_s^t \cdot \phi_s^t && \forall s \in S,\\
y_s &\leq \textstyle\sum_{t\in T} x_s^t \cdot \delta_s \cdot \pi_s^t && \forall s \in S,\\
w_1 &= \textstyle\sum_{i\in I} b_i \cdot \kappa_i \cdot \omega && ,\\
w_s &= z_s + y_s && \forall s \in S,\\
(\mathcal{P}_{\text{X.3}}) \qquad w_s &\leq \textstyle\sum_{i\in I} b_i \cdot \kappa_i \cdot \omega && \forall s \in S,\\
w_s &\geq \textstyle\sum_{i\in I} b_i \cdot \kappa_i \cdot \zeta + \nu_s && \forall s \in S,\\
v &\leq z_s && \forall s \in S,\\
\textstyle\sum_{i\in I} b_i &= 1 && ,\\
\textstyle\sum_{t\in T} x_s^t &\leq 1 && \forall s \in S,\\
x_s^t &= x_{s-N}^t && \forall t \in T, \forall s \in S, s > N,\\
x_s^{TFS} &= 1 && \forall s \in S^{TFS},\\
x_s^{TFS} &= 0 && \forall s \in S\backslash S^{TFS},
\end{aligned}
$$

$$
\begin{aligned}
x_d^t &\leq \tfrac{1}{2}\textstyle\sum_{s\in S_d} x_s^t && \forall t \in T,\ \forall d \in D,\\
h_{dwell,1} &= \tfrac{1}{2}\left(\textstyle\sum_{i\in I} b_i \cdot \kappa_i + w_A - \nu_A\right)\cdot \delta_{depot} && ,\\
h_{dwell,s} &= \tfrac{1}{2}(z_s + w_s)\cdot \delta_s && \forall s \in S\backslash\{1\},\\
h_{travel,s} &= \tfrac{1}{2}(w_s + z_{s+1})\cdot \tau_s && \forall s \in S\backslash\{A\},\\
h_{travel,A} &= \left(\textstyle\sum_{i\in I} b_i \cdot \kappa_i + w_A - \nu_A\right)\cdot \tau_{depot} && ,\\
DOD_i &\geq b_i - \frac{v}{\kappa_i} && \forall i \in I,\\
b_i - SOC_{avg,i} &\leq \frac{\sum_{j\in I} b_j \cdot \kappa_j}{\kappa_i} - \frac{\sum_{s\in S}\left[h_{dwell,s} + h_{travel,s}\right]}{\kappa_i \cdot \theta_{day}} && \forall i \in I,\\
(\mathcal{P}_{X.3}) \qquad x_s^t &\in \{0,1\} && \forall t \in T,\ \forall s \in S,\\
x_d^t &\in \{0,1\} && \forall t \in T,\ \forall d \in D,\\
b_i &\in \{0,1\} && \forall i \in I,\\
y_s &\geq 0 && \forall s \in S,\\
z_s &\geq 0 && \forall s \in S,\\
w_s &\geq 0 && \forall s \in S,\\
v &\geq 0 && ,\\
h_{j,s} &\geq 0 && \forall j \in \{dwell, travel\},\ \forall s \in S,\\
DOD_i &\geq 0 && \forall i \in I,\\
SOC_{avg,i} &\geq 0 && \forall i \in I.
\end{aligned}
$$

Appendix C

Calculus for Energy Consumption Integral

The integration of the power consumption equation is shown here. It is required to determine the energy consumption between two consecutive stops. The velocity of a bus is set to follow a speed profile over three phases, acceleration, constant speed and deceleration, expressed as follows.

$$s_{ij}^{I}(t) = r_a \cdot t, \qquad s_{ij}^{II}(t) = v, \qquad s_{ij}^{III}(t) = v - r_d \cdot t$$

The power consumption equation (4.2) is rewritten:

$$P_{i,j}(t) = A \cdot [s_{ij}(t)]^3 + B \cdot [s_{ij}(t)] + C \cdot \left|\frac{\mathrm{d}s_{ij}(t)}{\mathrm{d}t}\right| s_{ij}(t),$$

with

$$\begin{aligned} A &= \frac{\frac{1}{2}\rho_{air} A_f c_d}{\hat{\eta}} \\ B &= \frac{m_v g c_r}{\hat{\eta}} \\ C &= \frac{m_v}{\hat{\eta}}. \end{aligned}$$

The energy consumption integral is split in three separate integrals for the three different velocity phases.

Phase I - acceleration If we substitute the speed profile for phase I in the power consumption profile, we get the following.

$$P_{i,j}^{I}(t) = A r_a^3 \cdot t^3 + B r_a \cdot t + C r_a^2 \cdot t$$

Integrating over time gives us the following.

$$\begin{aligned} \int_0^{\tau_i^I} P_{i,j}^{I}(t)\mathrm{d}t &= \int_0^{\tau_i^I} A r_a^3 \cdot t^3 \mathrm{d}t + \int_0^{\tau_i^I} B r_a \cdot t \mathrm{d}t + \int_0^{\tau_i^I} C r_a^2 \cdot t \mathrm{d}t \\ &= [\tfrac{1}{4} A r_a^3 \cdot t^4]_0^{\tau_i^I} + [\tfrac{1}{2} B r_a \cdot t^2]_0^{\tau_i^I} + [\tfrac{1}{2} C r_a^2 \cdot t^2]_0^{\tau_i^I} \\ &= \tfrac{1}{4} A r_a^3 \cdot (\tau_i^I)^4 + (B + C r_a)(\tfrac{1}{2} r_a \cdot (\tau_i^I)^2) = \mu_i^I \end{aligned}$$

Phase II - constant speed If we substitute the speed profile for phase II in the power consumption profile, we get the following.

$$P_{i,j}^{II}(t) = A \cdot v^3 + B \cdot v + C \cdot 0$$

Integrating over time gives us the following.

$$\begin{aligned}\int_0^{\tau_i^{II}} P_{i,j}^{II}(t)\mathrm{d}t &= \int_0^{\tau_i^{II}} Av^3\mathrm{d}t + \int_0^{\tau_i^{II}} Bv\mathrm{d}t \\ &= [Av^3 \cdot t]_0^{\tau_i^{II}} + [Bv \cdot t]_0^{\tau_i^{II}} \\ &= (Av^2 + B)v \cdot \tau_i^{II} = \mu_i^{II}\end{aligned}$$

Phase III - deceleration If we substitute the speed profile for phase III in the power consumption profile, we get the following.

$$P_{i,j}^{III}(t) = A \cdot (v - r_d \cdot t)^3 + B \cdot (v - r_d \cdot t) + C \cdot |-r_d|(v - r_d \cdot t)$$

Integrating over time gives us the following.

$$\begin{aligned}\int_0^{\tau_i^{III}} P_{i,j}^{III}(t)\mathrm{d}t &= \int_0^{\tau_i^{III}} A(v - r_d \cdot t)^3\mathrm{d}t + \int_0^{\tau_i^{III}} B(v - r_d \cdot t)\mathrm{d}t + \int_0^{\tau_i^{III}} C(vr_d - r_d^2 \cdot t)\mathrm{d}t \\ &= \Big[-\frac{A}{4r_d}(v - r_d \cdot t)^4\Big]_0^{\tau_i^{III}} + [B(v - \tfrac{1}{2}r_d \cdot t)t]_0^{\tau_i^{III}} + [C(vr_d - \tfrac{1}{2}r_d^2 \cdot t)t]_0^{\tau_i^{III}} \\ &= \frac{Av^4}{4r_d} - \frac{A}{4r_d}(v - r_d \cdot \tau_i^{III})^4 + (B + Cr_d)((v - \tfrac{1}{2}r_d \cdot \tau_i^{III})\tau_i^{III}) = \mu_i^{III}\end{aligned}$$

Combining the three integrals we get the energy consumption for traveling from stop i to stop j:

$$\mu_i = \mu_i^I + \mu_i^{II} + \mu_i^{III}$$

Bibliography

Barco, John et al. (2017). "Optimal Routing and Scheduling of Charge for Electric Vehicles: A Case Study". In: *Mathematical Problems in Engineering* 2017.

Burke, Andrew and Marshall Miller (2011). "The power capability of ultracapacitors and lithium batteries for electric and hybrid vehicle applications". In: *Journal of Power Sources* 196.1, pp. 514–522.

Chankong, Vira and Yacov Y. Haimes (1983). *Multiobjective Decision Making: Theory and Methodology*. Elsevier Science Publishing Co., New York, NY.

Chao, Zhu and Chen Xiaohong (2013). "Optimizing battery electric bus transit vehicle scheduling with battery exchanging: Model and case study". In: *Procedia-Social and Behavioral Sciences* 96, pp. 2725–2736.

Chen, Jingmin et al. (2013). "Planning of feeding station installment for electric urban public mass-transportation system". In: *13^{th} Swiss Transportation Research Conference*. Paper no. EPFL-CONF-195881.

Chen, Min and Gabriel A. Rincon-Mora (2006). "Accurate Electrical Battery Model Capable of Predicting Runtime and *I-V* Performance". In: *IEEE Transactions on Energy Conversion* 21.2, pp. 504–511.

Ding, Huajie, Zechun Hu, and Yonghua Song (2015). "Value of the energy storage system in an electric bus fast charging station". In: *Applied Energy* 157, pp. 630–639.

Dueker, Kenneth J et al. (2004). "Determinants of bus dwell time". In: *Journal of Public Transportation* 7.1, p. 2.

Ecker, Madeleine et al. (2014). "Calendar and cycle life study of Li(NiMnCo)O_2-based 18650 lithium-ion batteries". In: *Journal of Power Sources* 248, pp. 839–851.

Ehrgott, Matthias (2006). *Multicriteria Optimization*. Springer Science & Business Media.

Feng, Wei and Miguel Figliozzi (2013). "An economic and technological analysis of the key factors affecting the competitiveness of electric commercial vehicles: A case study from the USA market". In: *Transportation Research Part C: Emerging Technologies* 26, pp. 135–145.

Fernández, Rodrigo et al. (2010). "Influence of platform height, door width, and fare collection on bus dwell time: laboratory evidence for Santiago de Chile". In: *Transportation Research Record: Journal of the Transportation Research Board* 2143, pp. 59–66.

Haimes, Yacov Y., Leon S. Lasdon, and D. A. Wismer (1971). "On a Bicriterion Formulation of the Problems of Integrated System Identification and System Optimization". In: *IEEE Transactions on Systems, Man, and Cybernetics* 1.3, pp. 296–297.

Han, Sekyung, Soohee Han, and Hirohisa Aki (2014). "A practical battery wear model for electric vehicle charging applications". In: *Applied Energy* 113, pp. 1100–1108.

Hoke, Anderson et al. (2011). "Electric Vehicle Charge Optimization Including Effects of Lithium-Ion Battery Degradation". In: *Vehicle Power and Propulsion Conference (VPPC)*. IEEE.

Hu, Xiaosong et al. (2013). "Energy Efficiency Analysis of a Series Plug-In Hybrid Electric Bus with Different Energy Management Strategies and Battery Sizes". In: *Applied Energy* 111, pp. 1001–1009.

Kameda, Hisashi and Naoto Mukai (2011). "Optimization of charging station placement by using taxi probe data for on-demand electrical bus system". In: *International Conference on Knowledge-Based and Intelligent Information and Engineering Systems*. Springer, pp. 606–615.

Korsesthakarn, Kanticha and Angkee Sripakagorn (2014). "Implementation of energy storage system with fleet management on electric shuttle buses". In: *Energy Procedia* 61, pp. 1929–1932.

Kunith, Alexander, Roman Mendelevitch, and Dietmar Goehlich (2017). "Electrification of a city bus network—An optimization model for cost-effective placing of charging infrastructure and battery sizing of fast-charging electric bus systems". In: *International Journal of Sustainable Transportation* 11.10, pp. 707–720.

Lajunen, Antti (2014). "Energy consumption and cost-benefit analysis of hybrid and electric city buses". In: *Transportation Research Part C: Emerging Technologies* 38, pp. 1–15.

Larminie, James and John Lowry (2012). *Electric Vehicle Technology Explained*. 2nd. John Wiley & Sons, Inc.

Liu, Wei (2013). *Introduction to Hybrid Vehicle System Modeling and Control*. John Wiley & Sons.

Lodi, G., R. Manzoni, and G. Crugnola (2010). "Batteries for full electric and hybrid buses: fleet operation results and relevant battery improvements". In: *The 25th World Battery Hybrid and Fuel Cell Electric Vehicle Symposium and Exhibition, Shenzen, China*.

Lyon, Thomas P et al. (2012). "Is "smart charging" policy for electric vehicles worthwhile?" In: *Energy Policy* 41, pp. 259–268.

Marano, Vincenzo et al. (2009). "Lithium-ion Batteries Life Estimation for Plug-in Hybrid Electric Vehicles". In: *Vehicle Power and Propulsion Conference*. IEEE, pp. 536–543.

Markel, Tony, Kandler Smith, and Ahmad A. Pesaran (2009). "Improving Petroleum Displacement Potential of PHEVs Using Enhanced Charging Scenarios". In: *Electric and Hybrid Vehicles Power Sources, Models, Sustainability, Infrastructure and the Market*. Elsevier. Chap. 8, pp. 211–225.

Marra, Francesco et al. (2012). "Demand Profile Study of Battery Electric Vehicle under Different Charging Options". In: *Power and Energy Society General Meeting*. IEEE, pp. 1–7.

Montoya, Alejandro et al. (2017). "The electric vehicle routing problem with nonlinear charging function". In: *Transportation Research Part B: Methodological* 103, pp. 87–110.

Moura, Scott Jason et al. (2011). "A Stochastic Optimal Control Approach for Power Management in Plug-In Hybrid Electric Vehicles". In: *IEEE Transactions on control systems technology* 19.3, pp. 545–555.

Omar, Noshin et al. (2014). "Lithium iron phosphate based battery – Assessment of the aging parameters and development of cycle life model". In: *Applied Energy* 113, pp. 1575–1585.

Pelletier, Samuel et al. (2017). "Battery degradation and behaviour for electric vehicles: Review and numerical analyses of several models". In: *Transportation Research Part B: Methodological* 103, pp. 158–187.

Peterson, Scott B., Jay Apt, and J. F. Whitacre (2010). "Lithium-ion battery cell degradation resulting from realistic vehicle and vehicle-to-grid utilization". In: *Journal of Power Sources* 195.8, pp. 2385–2392.

Pihlatie, Mikko, S Kukkonen, et al. (2014). "Fully electric city buses-The viable option". In: *Electric Vehicle Conference (IEVC), 2014 IEEE International*. IEEE, pp. 1–8.

Pihlatie, Mikko and Marko Paakkinen (2017). "Requirements and Technology for Electric Bus Fast Charging Infrastructure". In: *International Conference Electric Mobility and Public Transport*. VTT Research.

Rahmoun, Ahmad and Helmuth Biechl (2012). "Modelling of Li-ion batteries using equivalent circuit diagrams". In: *Przegląd Elektrotechniczny (Electrical review)* 88.7b, pp. 152–156.

Rogelj, Joeri et al. (2016). "Paris Agreement climate proposals need a boost to keep warming well below 2 °C". In: *Nature* 534.7609, pp. 631–639.

Rogge, Matthias, Sebastian Wollny, and Dirk Uwe Sauer (2015). "Fast Charging Battery Buses for the Electrification of Urban Public Transport-A Feasibility Study Focusing on Charging Infrastructure and Energy Storage Requirements". In: *Energies* 8.5, pp. 4587–4606.

Rosenkranz, Christian (2003). "Deep-cycle batteries for plug-in hybrid application". In: *20th International Electric Vehicle Symposium and Exposition (EVS-20), Long Beach, California*.

Santini, D. J., K. G. Gallagher, and P. A. Nelson (2010). "Modeling of Manufacturing Costs of Lithium-Ion Batteries for HEVs, PHEVs, and EVs". In: *25th World Battery, Hybrid and Fuel Cell Electric Vehicle Symposium and Exhibition (EVS-25), Shenzhen, China*.

Sarasketa-Zabala, E. et al. (2015). "Cycle ageing analysis of a $LiFePO_4$/graphite cell with dynamic model validations: Towards realistic lifetime predictions". In: *Journal of Power Sources* 275, pp. 573–587.

Scrosati, Bruno and Jürgen Garche (2010). "Lithium batteries: Status, prospects and future". In: *Journal of Power Sources* 195.9, pp. 2419–2430.

Smith, Kandler et al. (2010). *Design of Electric Drive Vehicle Batteries for Long Life and Low Cost: Robustness to Geographic and Consumer-Usage Variation (Presentation)*. Tech. rep. National Renewable Energy Laboratory (NREL), Golden, CO.

Spotzi B.V. and TomTom (2013). *Speed profile road network map*. URL: `https://www.spotzi.com/nl/kaarten/straten/verkeerssnelheden-nederland/`.

Sweda, Timothy M., Irina S. Dolinskaya, and Diego Klabjan (2017). "Optimal Recharging Policies for Electric Vehicles". In: *Transportation Science* 51.2, pp. 457–479.

Tirachini, Alejandro (2013). "Bus dwell time: the effect of different fare collection systems, bus floor level and age of passengers". In: *Transportmetrica A: Transport Science* 9.1, pp. 28–49.

Tremblay, Olivier, Louis-A. Dessaint, and Abdel-Illah Dekkiche (2007). "A Generic Battery Model for the Dynamic Simulation of Hybrid Electric Vehicles". In: *Vehicle Power and Propulsion Conference (VPPC)*. IEEE, pp. 284–289.

Van Vliet, Oscar P. R. et al. (2010). "Techno-economic comparison of series hybrid, plug-in hybrid, fuel cell and regular cars". In: *Journal of power sources* 195.19, pp. 6570–6585.

Wang, John et al. (2011). "Cycle-life model for graphite-$LiFePO_4$ cells". In: *Journal of Power Sources* 196.8, pp. 3942–3948.

Wang, Lijuan et al. (2015). "A Cost Effectiveness Analysis of Quasi-Static Wireless Power Transfer for Plug-In Hybrid Electric Transit Buses". In: *Vehicle Power and Propulsion Conference (VPPC)*. IEEE, pp. 1–7.

Wehres, Ulrich et al. (2016). "Modeling Uncertainty for a Catenary-free Electrical Bus". In: *16th Swiss Transportation Research Conference*. Paper no. EPFL-CONF-218674.

Weiss, Martin et al. (2012). "On the electrification of road transport – Learning rates and price forecasts for hybrid-electric and battery-electric vehicles". In: *Energy Policy* 48, pp. 374–393.

Wood, Eric, Marcus Alexander, and Thomas H. Bradley (2011). "Investigation of battery end-of-life conditions for plug-in hybrid electric vehicles". In: *Journal of Power Sources* 196.11, pp. 5147–5154.

World Resources Institute (2013). *Climate Analysis Indicators Tool*. URL: `http://cait.wri.org`.

Xu, Bolun (2013). "Degradation-limiting Optimization of Battery Energy Storage Systems Operation". MA thesis. Eidgenössische Technische Hochschule, Zürich, Switzerland.

Zheng, Minxin, Bojin Qi, and Xiaowei Du (2009). "Dynamic model for characteristics of Li-ion battery on electric vehicle". In: *4th IEEE Conference on Industrial Electronics and Applications (ICIEA)*. IEEE, pp. 2867–2871.